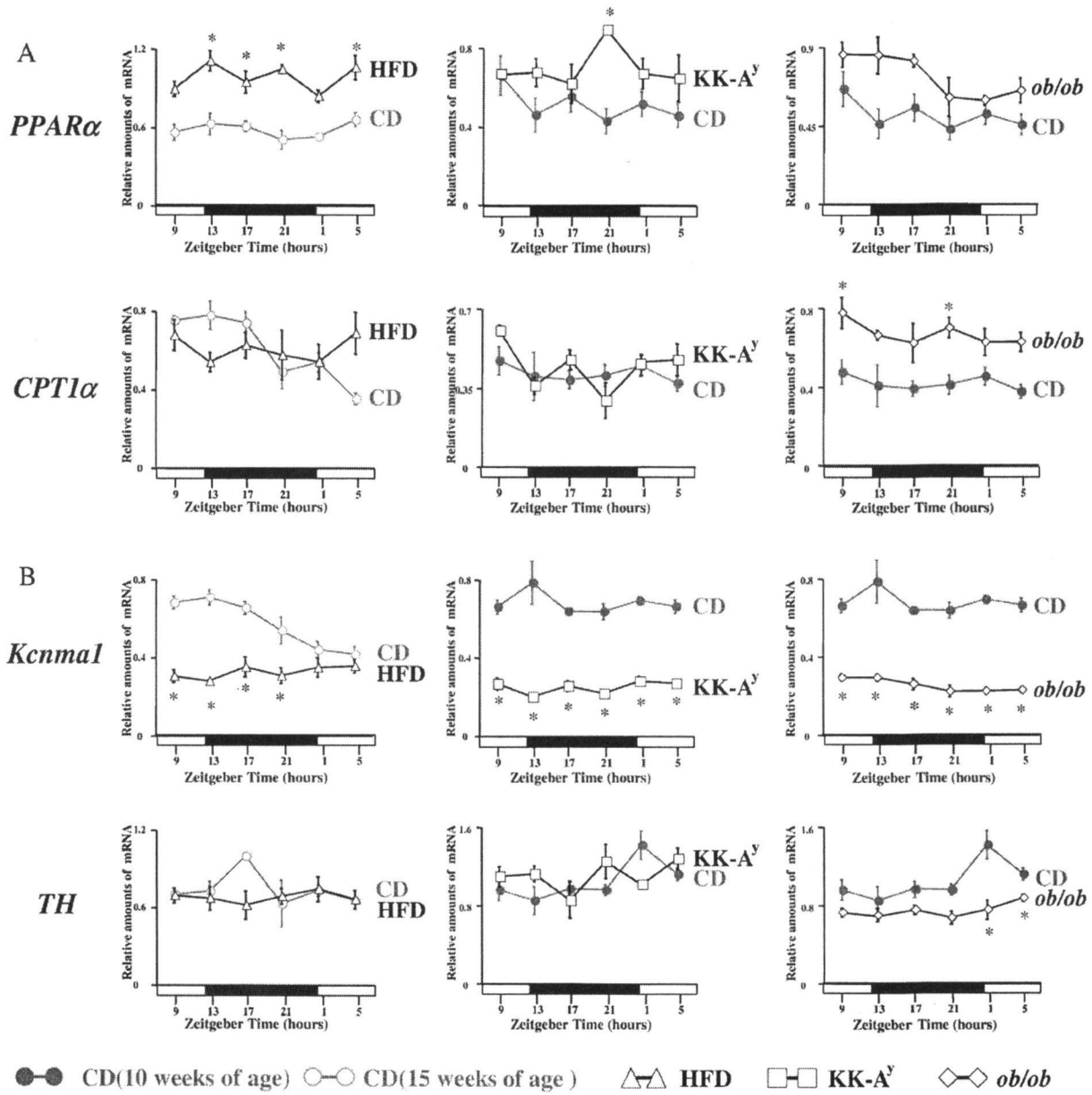

Fig. 4 – mRNA expression profiles of clock-related genes in NTS of obesity models. Daily mRNA expression profiles of PPARα and CPT1α (A), *Kcnma1* and *TH* (B) in the NTS of 10-week-old CD mice (●–●), 15-week-old CD mice (○–○), HFD mice (△–△), KK-A^y mice (□–□) and *ob/ob* mice (◇–◇). Data are presented as means ± SE (n = 4–5/group). *$P < 0.05$ by 2-way ANOVA followed by Tukey's post hoc test.

(CLEA Japan, Tokyo, Japan) information, KK-A^y mice were generated by crossing KK mice with C57BL/6-A^y mice. KK mice are mildly obese and insulin resistant (Ando et al., 2006); (Yamada et al., 2006). Therefore, as reported previously (Ando et al., 2006), to examine whether obesity per se alters circadian expressions of clock genes in the CNS, we used C57BL/6 mice, rather than KK mice, as lean controls for KK-A^y mice. Mice were housed individually and given a standard laboratory diet (65% carbohydrate, 4% fat, 24% protein) and water *ad libitum*. These animals, at 10 weeks of age, were sacrificed to obtain blood and brain samples at the following zeitgeber times (ZTs): 1, 5, 9, 13, 17 and 21, in which ZT 0 is defined as lights on and

Fig. 3 – Alterations in circadian mRNA expression profiles of *clock* genes in NTS of obesity models Daily mRNA expression profiles of *clock* genes in the NTS of 10-week-old CD mice (●–●), 15-week-old CD mice (○–○), HFD mice (△–△), KK-A^y mice (□–□) and *ob/ob* mice (◇–◇). Data are presented as means ± SE (n = 4–5/group). *$P < 0.05$ by 2-way ANOVA followed by Tukey's post hoc test.

Table 1 – Sequences of quantitative RT-PCR primers

Gene	Primer 1	Primer 2
Clock	5′-agatcagttcaatgtcctca-3′	5′-tgtcgaatctcactagcatc-3′
Bmal1	5′-cgtcgggacaaaatgaaca-3′	5′-ttctgtgtatgggttggtgg-3′
Npas2	5′-cagcagccaccaccctatt-3′	5′-tgcggaggtgtagactgtgt-3′
Per1	5′-gtactttggcagcatcgactc-3′	5′-cggtcttgcttcagcacaga-3′
Per2	5′-cagccaccctgaaaagga-3′	5′-gtgagggacaccacactctc-3′
Cry1	5′-cggtggaaattgctctca-3′	5′-ggcatcctcttcctgacta-3′
Rev-erbα	5′-aactccctggcacttacc-3′	5′-gttcttcagcaccagagc-3′
PPARα	5′-tccctgtttgtggctgctat-3′	5′-ttgggaagaggaaggtgtca-3′
CPT1α	5′-gagccatgaagccctcaaacagat-3′	5′-gctgtacaacatgggctttcgacc-3′
Kcnma1	5′-ggatggtggttgttatggtg-3′	5′-tcgtagggaggattggtgat-3′
TH	5′-ggctgctgtcttcctatggaga-3′	5′-atgggcgctggatacgaga-3′
GAPDH	5′-tgaaggtcggtgtgaacg-3′	5′-ccattctcggccttgact-3′

PPARα, peroxisome proliferator-activated receptor α
CPT1α, carnitine palmitoyl-transferase-1α
TH, tyrosine hydroxylase
GAPDH, glyceraldehyde-3-phosphate dehydrogenase

ZT 12 as light off. High-fat-chow feeding (32% safflower oil, 33.1% casein, 17.6% sucrose, and 5.6% cellulose) (Yamada et al., 2006) was initiated at 5 weeks of age in C57BL/6 mice and continued for 10 weeks. All animal studies were conducted in accordance with the institutional guidelines for animal experiments at Tohoku University.

4.2. *Blood analysis*

Blood glucose and serum insulin, leptin, and free fatty acid levels were determined as previously described (Yamada et al., 2006).

4.3. *Tissue preparation*

All animals were sacrificed by decapitation at the indicated ZTs. The brains were immediately frozen in isopentane on dry ice and stored at-80 °C until RNA purification.

4.4. *Laser micro-dissection*

Coronal cryostat sections (20 μm) through the bilateral NTS at the level of the area postrema (Fig. 1A) were placed on PEN-coated slides (Leica Microsystems). Laser micro-dissection was carried out on a Leica AS LMD (Leica Microsystems). Immediately after micro-dissection, the samples were placed on dry ice and then stored at a-80 °C until RNA purification.

4.5. *RNA purification and quantitative real-time PCR (qRT-PCR)*

Total RNA was purified from 10 20-micron laser micro-dissected NTS specimens with an RNeasy microkit (QIAGEN, Valencia, CA, USA), and cDNA synthesized from total RNA was evaluated with a real-time PCR quantitative system (Light Cycler Quick System 350S; Roche Diagnostics GmbH, Mannheim, Germany) as previously reported (Yamada et al., 2006).The relative amount of mRNA was calculated with GAPDH mRNA as the invariant control. The primers used are shown in Table 1.

4.6. *Statistics*

The results are presented as means ± SE. Body weights and time-series data were analyzed by 1-way ANOVA to determine significant differences. The statistical significance of differences between two groups was determined using 2-way ANOVA followed by Tukey's post hoc test.

Acknowledgments

We thank Ms. I. Sato, J. Fushimi, K. Aizawa and T. Takasugi for technical support. This work was supported by Grants-in-Aid for Scientific Research (B2, 15390282) to H.K. from the Japanese Ministry of Education, Science, Sports and Culture, and a Grant-in-Aid for Scientific Research (H19-genome-005) to Y.O. from the Japanese Ministry of Health, Labor and Welfare. This work was also supported by the Global-COE Program to Y.O. and the 21st Century COE Program to H.K. from the Japanese Ministry of Education, Science, Sports and Culture.

REFERENCES

Ando, H., Yanagihara, H., Hayashi, Y., Obi, Y., Tsuruoka, S., Takamura, T., Kaneko, S., Fujimura, A., 2005. Rhythmic messenger ribonucleic acid expression of clock genes and adipocytokines in mouse visceral adipose tissue. Endocrinology 146, 5631–5636.

Ando, H., Oshima, Y., Yanagihara, H., Hayashi, Y., Takamura, T., Kaneko, S., Fujimura, A., 2006. Profile of rhythmic gene expression in the livers of obese diabetic KK-A(y) mice. Biochem. Biophys. Res. Commun. 346, 1297–1302.

Badman, M.K., Flier, J.S., 2005. The gut and energy balance: visceral allies in the obesity wars. Science 307, 1909–1914.

Canaple, L., Rambaud, J., Dkhissi-Benyahya, O., Rayet, B., Tan, N.S., Michalik, L., Delaunay, F., Wahli, W., Laudet, V., 2006.

Reciprocal regulation of brain and muscle Arnt-like protein 1 and peroxisome proliferator-activated receptor alpha defines a novel positive feedback loop in the rodent liver circadian clock. Mol. Endocrinol. 20, 1715–1727.
Chawla, A., Lazar, M.A., 1993. Induction of Rev-ErbA alpha, an orphan receptor encoded on the opposite strand of the alpha-thyroid hormone receptor gene, during adipocyte differentiation. J. Biol. Chem. 268, 16265–16269.
Danguir, J., 1989. Sleep patterns in the genetically obese Zucker rat: effect of acarbose treatment. Am. J. Physiol. 256, R281–283.
Date, Y., Shimbara, T., Koda, S., Toshinai, K., Ida, T., Murakami, N., Miyazato, M., Kokame, K., Ishizuka, Y., Ishida, Y., Kageyama, H., Shioda, S., Kangawa, K., Nakazato, M., 2006. Peripheral ghrelin transmits orexigenic signals through the noradrenergic pathway from the hindbrain to the hypothalamus. Cell. Metab. 4, 323–331.
Dunlap, J.C., 2006. Physiology. Running a clock requires quality time together. Science 311, 184–186.
Flier, J.S., 2004. Obesity wars: molecular progress confronts an expanding epidemic. Cell 116, 337–350.
Grill, H.J., 2006. Distributed neural control of energy balance: contributions from hindbrain and hypothalamus. Obesity (Silver Spring) 14 (Suppl. 5), 216S–221S.
Herichova, I., Mravec, B., Stebelova, K., Krizanova, O., Jurkovicova, D., Kvetnansky, R., Zeman, M., 2007. Rhythmic clock gene expression in heart, kidney and some brain nuclei involved in blood pressure control in hypertensive TGR(mREN-2)27 rats. Mol. Cell. Biochem. 296, 25–34.
Hermes, S.M., Mitchell, J.L., Aicher, S.A., 2006. Most neurons in the nucleus tractus solitarii do not send collateral projections to multiple autonomic targets in the rat brain. Exp. Neurol. 198, 539–551.
Jenkins, J.B., Omori, T., Guan, Z., Vgontzas, A.N., Bixler, E.O., Fang, J., 2006. Sleep is increased in mice with obesity induced by high-fat food. Physiol. Behav. 87, 255–262.
Katagiri, H., Yamada, T., Oka, Y., 2007. Adiposity and cardiovascular disorders: disturbance of the regulatory system consisting of humoral and neuronal signals. Circ. Res. 101, 27–39.
Kohsaka, A., Laposky, A.D., Ramsey, K.M., Estrada, C., Joshu, C., Kobayashi, Y., Turek, F.W., Bass, J., 2007. High-fat diet disrupts behavioral and molecular circadian rhythms in mice. Cell. Metab. 6, 414–421.
Kudo, T., Akiyama, M., Kuriyama, K., Sudo, M., Moriya, T., Shibata, S., 2004. Night-time restricted feeding normalises clock genes and Pai-1 gene expression in the db/db mouse liver Diabetologia 47, 1425–1436.
Laposky, A.D., Shelton, J., Bass, J., Dugovic, C., Perrino, N., Turek, F. W., 2006. Altered sleep regulation in leptin-deficient mice. Am. J. Physiol., Regul. Integr. Comp. Physiol. 290, R894–903.
Lara, J., Acevedo, J.J., Onetti, C.G., 1999. Large-conductance Ca2+-activated potassium channels in secretory neurons. J. Neurophysiol. 82, 1317–1325.
Lovell, P.V., McCobb, D.P., 2001. Pituitary control of BK potassium channel function and intrinsic firing properties of adrenal chromaffin cells. J. Neurosci. 21, 3429–3442.
McClung, C.A., Sidiropoulou, K., Vitaterna, M., Takahashi, J.S., White, F.J., Cooper, D.C., Nestler, E.J., 2005. Regulation of dopaminergic transmission and cocaine reward by the Clock gene. Proc. Natl. Acad. Sci. U. S. A. 102, 9377–9381.
Megirian, D., Dmochowski, J., Farkas, G.A., 1998. Mechanism controlling sleep organization of the obese Zucker rats. J. Appl. Physiol. 84, 253–256.
Memon, R.A., Tecott, L.H., Nonogaki, K., Beigneux, A., Moser, A.H., Grunfeld, C., Feingold, K.R., 2000. Up-regulation of peroxisome proliferator-activated receptors (PPAR-alpha) and PPAR-gamma messenger ribonucleic acid expression in the liver in murine obesity: troglitazone induces expression of PPAR-gamma-responsive adipose tissue-specific genes in the liver of obese diabetic mice. Endocrinology 141, 4021–4031.
Menetrey, D., Basbaum, A.I., 1987. Spinal and trigeminal projections to the nucleus of the solitary tract: a possible substrate for somatovisceral and viscerovisceral reflex activation. J. Comp. Neurol. 255, 439–450.
Menetrey, D., De Pommery, J., 1991. Origins of spinal ascending pathways that reach central areas involved in visceroception and visceronociception in the rat. Eur. J. Neurosci. 3, 249–259.
Meredith, A.L., Wiler, S.W., Miller, B.H., Takahashi, J.S., Fodor, A.A., Ruby, N.F., Aldrich, R.W., 2006. BK calcium-activated potassium channels regulate circadian behavioral rhythms and pacemaker output. Nat. Neurosci. 9, 1041–1049.
Moreno, S., Farioli-Vecchioli, S., Ceru, M.P., 2004. Immunolocalization of peroxisome proliferator-activated receptors and retinoid X receptors in the adult rat CNS. Neuroscience 123, 131–145.
Panda, S., Antoch, M.P., Miller, B.H., Su, A.I., Schook, A.B., Straume, M., Schultz, P.G., Kay, S.A., Takahashi, J.S., Hogenesch, J.B., 2002. Coordinated transcription of key pathways in the mouse by the circadian clock. Cell 109, 307–320.
Prasai, M.J., George, J.T., Scott, E.M., 2008. Molecular clocks, type 2 diabetes and cardiovascular disease. Diab. Vasc. Dis. Res. 5, 89–95.
Preitner, N., Damiola, F., Lopez-Molina, L., Zakany, J., Duboule, D., Albrecht, U., Schibler, U., 2002. The orphan nuclear receptor REV-ERBalpha controls circadian transcription within the positive limb of the mammalian circadian oscillator. Cell 110, 251–260.
Ramsey, K.M., Marcheva, B., Kohsaka, A., Bass, J., 2007. The clockwork of metabolism. Annu. Rev. Nutr. 27, 219–240.
Reick, M., Garcia, J.A., Dudley, C., McKnight, S.L., 2001. NPAS2: an analog of clock operative in the mammalian forebrain. Science 293, 506–509.
Ritter, S., Watts, A.G., Dinh, T.T., Sanchez-Watts, G., Pedrow, C., 2003. Immunotoxin lesion of hypothalamically projecting norepinephrine and epinephrine neurons differentially affects circadian and stressor-stimulated corticosterone secretion. Endocrinology 144, 1357–1367.
Rudic, R.D., McNamara, P., Curtis, A.M., Boston, R.C., Panda, S., Hogenesch, J.B., Fitzgerald, G.A., 2004. BMAL1 and CLOCK, two essential components of the circadian clock, are involved in glucose homeostasis. PLoS Biol. 2, e377.
Sandoval, D., Cota, D., Seeley, R.J., 2008. The integrative role of CNS fuel-sensing mechanisms in energy balance and glucose regulation. Annu. Rev. Physiol. 70, 513–535.
Schibler, U., Sassone-Corsi, P., 2002. A web of circadian pacemakers. Cell 111, 919–922.
Schwartz, G.J., 2006. Integrative capacity of the caudal brainstem in the control of food intake. Philos. Trans. R. Soc. Lond., B Biol. Sci. 361, 1275–1280.
Staels, B., 2006. When the clock stops ticking, metabolic syndrome explodes. Nat Med. 12, 54–55 discussion 55.
Turek, F.W., Joshu, C., Kohsaka, A., Lin, E., Ivanova, G., McDearmon, E., Laposky, A., Losee-Olson, S., Easton, A., Jensen, D.R., Eckel, R.H., Takahashi, J.S., Bass, J., 2005. Obesity and metabolic syndrome in circadian Clock mutant mice. Science 308, 1043–1045.
Uno, K., Katagiri, H., Yamada, T., Ishigaki, Y., Ogihara, T., Imai, J., Hasegawa, Y., Gao, J., Kaneko, K., Iwasaki, H., Ishihara, H., Sasano, H., Inukai, K., Mizuguchi, H., Asano, T., Shiota, M., Nakazato, M., Oka, Y., 2006. Neuronal pathway from the liver modulates energy expenditure and systemic insulin sensitivity. Science 312, 1656–1659.
Yamada, T., Oka, Y., Katagiri, H., 2008. Inter-organ metabolic communication involved in energy homeostasis: potential therapeutic targets for obesity and metabolic syndrome. Pharmacol. Ther. 117, 188–198.

Yamada, T., Katagiri, H., Ishigaki, Y., Ogihara, T., Imai, J., Uno, K., Hasegawa, Y., Gao, J., Ishihara, H., Niijima, A., Mano, H., Aburatani, H., Asano, T., Oka, Y., 2006. Signals fromintra-abdominal fat modulate insulin and leptin sensitivity through different mechanisms: neuronal involvement in food-intake regulation. Cell. Metab. 3, 223–229.

Yang, Q., Graham, T.E., Mody, N., Preitner, F., Peroni, O.D., Zabolotny, J.M., Kotani, K., Quadro, L., Kahn, B.B., 2005. Serum retinol binding protein 4 contributes to insulin resistance in obesity and type 2 diabetes. Nature 436, 356–362.

Yang, X., Downes, M., Yu, R.T., Bookout, A.L., He, W., Straume, M., Mangelsdorf, D.J., Evans, R.M., 2006. Nuclear receptor expression links the circadian clock to metabolism. Cell 126, 801–810.

Neuroscience Research 64 (2009) 213–230

Contents lists available at ScienceDirect

Neuroscience Research

journal homepage: www.elsevier.com/locate/neures

Wolfram syndrome 1 (*Wfs1*) mRNA expression in the normal mouse brain during postnatal development

June Kawano [a,b,*], Ryutaro Fujinaga [b], Kiwako Yamamoto-Hanada [b], Yoshitomo Oka [c,d], Yukio Tanizawa [c], Koh Shinoda [b]

[a] *Laboratory for Neuroanatomy, Department of Neurology, Kagoshima University Graduate School of Medical and Dental Sciences, Kagoshima, 890-8544, Japan*
[b] *Division of Neuroanatomy, Department of Neuroscience, Yamaguchi University School of Medicine, Ube, Yamaguchi, 755-8505, Japan*
[c] *Division of Endocrinology, Metabolism, Hematological Sciences and Therapeutics, Department of Bio-Signal Analysis, Yamaguchi University Graduate School of Medicine, Ube, Yamaguchi, 755-8505, Japan*
[d] *Division of Molecular Metabolism and Diabetes, Tohoku University Graduate School of Medicine, Sendai, Miyagi, 980-8575, Japan*

ARTICLE INFO

Article history:
Received 28 August 2008
Received in revised form 28 February 2009
Accepted 4 March 2009
Available online 20 March 2009

Keywords:
Wolframin
CA1 field
Parasubiculum
Entorhinal cortex
Facial nucleus
Diabetes insipidus
Sensorineural hearing loss
In situ hybridization histochemistry

ABSTRACT

Wolfram syndrome is a rare genetic disorder accompanying diabetes insipidus, sensorineural hearing loss, neurological complications, and psychiatric illness. This syndrome has been attributed to mutations in the *WFS1* gene. In this study, we made a detailed histochemical analysis of the distribution of *Wfs1* mRNA in the brain of developing mice. There were three patterns of change in the strength of *Wfs1* mRNA signals from birth to early adulthood. In type 1, the signals were weak or absent in neonates but strong or moderate in young adults. This pattern was observed in the CA1 field, parasubiculum, and entorhinal cortex. In type 2, the signals were of a relatively constant strength during development. This pattern was seen in limbic structures (e.g. subiculum and central amygdaloid nucleus) and brainstem nuclei (e.g. facial and chochlear nuclei). In type 3, the signals peaked in the second week of age. This pattern was observed in the thalamic reticular nucleus. Thus, *Wfs1* mRNA was widely distributed in the normal mouse brain during postnatal development. This evidence may provide clues as to the physiological role of the *Wfs1* gene in the central nervous system, and help to explain endocrinological, otological, neurological, and psychiatric symptoms in Wolfram syndrome patients.

1. Introduction

Wolfram syndrome (OMIM 222300) is an autosomal recessive neurodegenerative disorder defined by young-onset non-autoimmune insulin-dependent diabetes mellitus and progressive optic atrophy (Wolfram and Wagener, 1938; Minton et al., 2003). The nuclear gene responsible for Wolfram syndrome has been identified as *WFS1* (Wolfram syndrome 1; Inoue et al., 1998; Strom et al., 1998), and is located at 4p16.1 (Polymeropoulos et al., 1994; Collier et al., 1996). The *WFS1* gene is also responsible for autosomal dominant low frequency sensorineural hearing loss (Bespalova et al., 2001; Young et al., 2001), and is a candidate to contribute low risk for type 2 diabetes mellitus (Minton et al., 2002; Sparsø et al., 2008; Wasson and Permutt, 2008). The WFS1 protein, also called wolframin, localizes primarily to the endoplasmic reticulum (ER) membrane, and contains nine transmembrane segments with the amino-terminus in the cytosol and the carboxy-terminus in the ER lumen (Takeda et al., 2001; Hofmann et al., 2003). Subsequent functional studies showed that the WFS1 protein is important in the regulation of intracellular Ca^{2+} homeostasis (Osman et al., 2003; Takei et al., 2006), contributes to cell cycle progression (Yamada et al., 2006), and is produced under conditions of troubled homeostasis, including ER stress (Yamaguchi et al., 2004; Fonseca et al., 2005; Ueda et al., 2005). In addition, screening for mutations in Wolfram syndrome patients demonstrated more than 50 distinct mutations of the *WFS1* gene, including stop, frameshift, deletion and missense mutations (Inoue et al., 1998; Strom et al., 1998; Hardy et al., 1999; Gómez-Zaera et al., 2001; Khanim et al., 2001; Tessa et al., 2001; Cano et al., 2007). Thus loss-of-function mutations in the *WFS1* gene have been linked to Wolfram syndrome, however, molecular functions of the WFS1 protein and the mechanism by which mutations of the *WFS1* gene cause Wolfram syndrome remain unclear.

* Corresponding author at: Laboratory for Neuroanatomy, Department of Neurology, Kagoshima University Graduate School of Medical and Dental Sciences, 35-1, Sakuragaoka 8-chome, Kagoshima, 890-8544, Japan. Tel.: +81 99 275 5212; fax: +81 99 275 5214.
E-mail address: kawanoj@m2.kufm.kagoshima-u.ac.jp (J. Kawano).

0168-0102/$ – see front matter © 2009 Elsevier Ireland Ltd and the Japan Neuroscience Society. All rights reserved.
doi:10.1016/j.neures.2009.03.005

Although the defining characteristics of Wolfram syndrome are diabetes mellitus (100%)[1] and optic atrophy (100%), other symptoms include cranial diabetes insipidus (73%), sensorineural deafness (62%), neurological complications (cerebellar ataxia and myoclonus; 62%), and psychiatric illness (60%) (Swift et al., 1990; Barrett et al., 1995). Accordingly, the term DIDMOAD (diabetes insipidus, diabetes mellitus, optic atrophy, and deafness) is used to describe Wolfram syndrome with more widespread complications (Barrett et al., 1995). The prevalence of Wolfram syndrome is one per 770,000 in the UK population, and the median age at death (commonly central respiratory failure with brainstem atrophy) is 30 years (range 25–49 years) (Barrett et al., 1995). Neuroradiological (Rando et al., 1992; Scolding et al., 1996; Ito et al., 2007) and neuropathological (Genís et al., 1997; Shannon et al., 1999) studies have reported severe atrophy in the brainstem, cerebellum, and optic nerve of Wolfram syndrome patients. Mild atrophy was also observed in the cerebral cortex and hypothalamus. Thus, clinical and pathological facts concerning brain-related (ophthalmological, endocrinological, otological, neurological, and psychiatric) symptoms in Wolfram syndrome have been accumulated. However, the site of pathology for these symptoms remains unclear. To obtain insights into the site of pathology for the symptoms, it is necessary to examine *WFS1* expression in the brain not only at the adult stage, but also at the developmental stages, since there is a possibility that lack of *WFS1* expression during development contributes to the progression of the brain-related symptoms of Wolfram syndrome caused by loss-of-function mutations in the *WFS1* gene. Insights into the site of pathology may provide hypotheses about the pathophysiology of the brain-related symptoms of Wolfram syndrome.

In the rodent brain, expression of the *Wfs1* gene has previously been described in the cerebral cortex, the basal ganglia, the hypothalamus, the brainstem motor and sensory nuclei, the reticular formation, and in the cerebellar cortex, as well as in the CA1 field of the hippocampus and in the amygdala (Takeda et al., 2001; Ishihara et al., 2004; Kato et al., 2008; Kawano et al., 2008; Luuk et al., 2008). To obtain neuroanatomical evidence for understanding the endocrinological, otological, neurological, and psychiatric symptoms of Wolfram syndrome, and to establish a basis for functional studies of the WFS1 protein in the brain, we performed a detailed histochemical analysis of the distribution of *Wfs1* mRNA signals in the brain of normal mice during postnatal development.

2. Materials and methods

2.1. Animals and tissue preparation

Male mice ($n = 10$; C57BL/6NCrlCrlj; Charles River Laboratories Japan, Inc., Yokohama, Kanagawa, Japan) were used in this study. The delivery day was designated as postnatal day 0 (P0). Three mice at 8 weeks old (P8W, early adulthood), two mice at P28, and five neonates at early postnatal ages, P0, P4, P7, P14, and P21, were used. Prior to the experiments, they were housed in an animal care facility with a 12-h light (lights on 8:00–20:00), 12-h dark photoperiod and free access to tap water and rodent chow. The mice were deeply anesthetized with sodium pentobarbital (50 mg/kg, i.p.), and perfused transcardially with 4% paraformaldehyde dissolved in 0.1 M sodium phosphate buffer (PB; pH 7.4) at 4 °C. Brains were removed from the skull, stored in the same fixative for 48 h, and then immersed in 30% saccharose in 0.1 M PB at 4 °C until they sank. The brains were frozen in powdered dry ice and coronally cut at a thickness of 40 μm. The sections were collected as a 1-in-5 series in a cryoprotectant medium (33.3% saccharose, 1% polyvinylpyrrolidone (K-30), and 33.3% ethylene glycol in 0.067 M sodium phosphate buffer (pH 7.4) containing 0.067% sodium azide; Warr et al., 1981) and stored at −30 °C prior to use. In each experimental case at ages P0 and P4, heads including the brain were processed as described above without decalcification.

All experimental protocols for this study were approved by the committee on the Ethics of Animal Experimentation at Yamaguchi University School of Medicine, and were conducted according to the guidelines for Animal Research of Yamaguchi University School of Medicine and The Law (No. 105) and Notification (No. 6) of the Japanese Government.

2.2. Preparation of cRNA probes

To synthesize a cRNA probe for *in situ* hybridization, a 1548-base fragment of the mouse *Wfs1* cDNA was amplified by RT-PCR, and subcloned into the vector pCR-Blunt (Invitrogen, Carlsbad, CA). The primers used were MOUSE-U2, 5′-T CCG TAC TCT CAC CGA CCT G-3′, and MOUSE L3, 5′-C TCA GGC GGC AGA CAG GAA T-3′. The fragment encoded the 3′-end of the protein-coding region including the stop codon, and occupied 85% of exon 8 where many mutations have been reported in the *WFS1* gene of Wolfram syndrome patients (Inoue et al., 1998; Strom et al., 1998; Hardy et al., 1999; Gómez-Zaera et al., 2001; Khanim et al., 2001; Cano et al., 2007). Two independent clones containing the insert with a different orientation (pCR-clone 19 for sense, pCR-clone 1 for anti-sense) were used. A sense or an anti-sense cRNA probe was obtained by in vitro transcription with a DIG RNA labeling kit (SP6/T7; Roche Diagnostics GmbH, Penzberg, Germany).

2.3. In situ hybridization histochemistry

In situ hybridization histochemistry was carried out as described previously (Kawano et al., 2008). Free-floating sections washed for 5 min in diethylpyrocarbonate-treated phosphate-buffered saline (DEPC-PBS) were pretreated with 0.2 N HCl for 20 min, washed twice for 5 min in DEPC-PBS, and then acetylated in 0.1 M triethanolamine–HCl (pH 8.0) containing 0.25% acetic anhydride for 10 min. Before the hybridization step, sections were washed again twice for 5 min with DEPC-PBS. All pretreatments were performed at 4 °C. Following the pretreatment, sections were preincubated in hybridization buffer (50% deionized-formamide; 10 mM Tris–HCl, pH 7.5; 1 mM EDTA, pH 8.0; 600 mM NaCl; 1× Denhardt's solution; 10% dextran sulfate; 0.25% sodium dodecyl sulfate; and 200 μg/ml yeast tRNA) at 55 °C for 1 h and then hybridized with DIG-labeled anti-sense cRNA probes (0.5 μg/ml; denatured at 95 °C for 5 min and cooled at 4 °C for 5 min shortly before use) in the same buffer at 55 °C for 16 h. After hybridization, the sections were washed with 2× SSC (300 mM NaCl, and 30 mM sodium citrate, pH 7.0) containing 50% formamide at 55 °C for 1 h, rinsed in wash buffer (500 mM NaCl, 10 mM Tris–HCl, pH 8.0, and 1 mM EDTA, pH 8.0) for 10 min and then incubated with RNase A (20 μg/ml; Sigma–Aldrich, St. Louis, MO) in wash buffer at 37 °C for 30 min. After being rinsed in wash buffer again for 10 min, they were soaked in 2× SSC containing 50% formamide and 0.2× SSC containing 50% formamide at 55 °C for 30 min each. To perform the immunoreaction, the sections were blocked in buffer 2 (buffer 1 (150 mM NaCl, and 100 mM Tris–HCl, pH 7.5) containing 2% blocking reagent) at 20 °C for 1 h and then incubated in buffer 2 containing alkaline phosphatase-conjugated sheep anti-DIG antibody (Roche Diagnostics) diluted 1:3000 at 20 °C for 16 h. After two washes in buffer 1 for 10 min, they were rinsed in buffer 3 (100 mM NaCl, 50 mM $MgCl_2$, and 100 mM Tris–HCl, pH 9.5) for 5 min and incubated with NBT/BCIP substrate (1:50; Roche Diagnostics) in buffer 3 at 37 °C for 2–4 h to visualize the immunocomplex. The coloring reaction was stopped with buffer 4 (1 mM EDTA, and 10 mM Tris–HCl, pH 8.0), and the sections were washed in

[1] Percentage in parentheses shows frequency of the feature in Wolfram syndrome patients.

phosphate-buffered saline, mounted on glass slides using a 0.6% gelatin solution, and air-dried. The slides were coverslipped with Entellan neu mountant (Merck KGaA, Darmstadt, Germany). As a control, a sense cRNA probe was used instead of the anti-sense cRNA probe. Few mRNA signals were observed in control sections. For the cytoarchitectonic analysis, adjacent series of brain sections at P0 and P8W (early adulthood) were subjected to Nissl staining by using cresyl violet (acetate) (Merck KGaA).

2.4. Photomicrographs and terminology

Brightfield photomicrographs were taken using a DXM1200 color digital camera (Nikon, Tokyo Japan) equipped with an Optiphot-2 photomicroscope (Nikon). Images were transferred to Adobe Photoshop 6 (Adobe Systems, San Jose, CA), and brightness, contrast, and picture sharpness were adjusted. No other adjustment was made.

The nomenclature used for the different regions of the brain primarily followed that of Paxinos and Franklin (2001).

3. Results

3.1. Changes in the strength of *Wfs1* mRNA expression during postnatal development

Postnatal changes in the strength of *Wfs1* mRNA expression in each of the mouse brain structures are shown in Table 1. A general

Table 1
Postnatal changes in the strength of *Wfs1* mRNA expression in each of the mouse brain structures.

		P0	P4	P7	P14	P28	Early adulthood (P8W)
Type 1a (expression is weak in neonates but strong in young adults)							
CA1	CA1 field of the hippocampus	+	++	++	+++	+++	+++
MEA	Medial entorhinal area	–	+	++	+++	+++	+++
LEA	Lateral entorhinal area	–	+	++	+++	+++	+++
PaS	Parasubiculum	–	–	+++	+++	+++	+++
Type 1b (expression is weak in neonates but moderate in young adults)							
MoCII	Layer II in the motor cortex	–	–	+	++	++	++
CgII	Layer II in the cingulate cortex	–	–	+	++	++	++
Pir	Piriform cortex	+	++	++	++	++	++
LS	Lateral septal nucleus	–	–	+	++	++	++
Acb	Nucleus accumbens	+	++	++	++	++	++
Me5	Mesencephalic trigeminal nucleus	+	+	+	+	+	++
7NM	Medial subdivision of the facial nucleus	+	+	+	+	++	++
Amb	Nucleus ambiguus	+	+	+	+	+	++
Type 1c (expression is absent in neonates but weak in young adults)							
SoCII	Layer II in the somatosensory cortex	–	–	–	+	+	+
AuCII	Layer II in the auditory cortex	–	–	–	+	+	+
ViCII	Layer II in the visual cortex	–	–	–	+	+	+
SC	Superior colliculus	–	–	–	+	+	+
Type 2a (expression is moderate and relatively constant throughout postnatal stages)							
S	Subiculum	++	++	++	++	++	++
Tu	Olfactory tuberculum	++	++	++	++	++	++
BSTL	Lateral bed nucleus of the stria terminalis	++	++	++	++	++	++
IPAC	Interstitial nucleus of the posterior limb of the anterior commissure	++	++	++	++	++	++
Ce	Central amygdaloid nucleus	++	++	++	++	++	++
CPu	Caudate putamen (caudal part)	++	++	++	++	++	++
Mo5	Motor nucleus of the trigeminal nerve	++	++	++	++	++	++
7NL	Lateral subdivision of the facial nucleus	++	++	++	++	++	++
12N	Hypoglossal nucleus	++	++	++	++	++	++
Type 2b (expression is weak and relatively constant throughout postnatal stages)							
MOB	Main olfactory bulb	+	+	+	+	+	+
AOB	Accessory olfactory bulb	+	+	+	+	+	+
SO	Supraoptic nucleus	+	+	+	+	+	+
PVNm	Magnocellular part of the paraventricular hypothalamic nucleus	+	+	+	+	+	+
IC	Inferior colliculus	+	+	+	+	+	+
LC	Nucleus coeruleus	+	+	+	+	+	+
DR	Dorsal raphe nucleus	+	+	+	+	+	+
MnR	Median raphe nucleus	+	+	+	+	+	+
Co	Cochlear nucleus	+	+	+	+	+	+
BSRt	Brainstem reticular formation	+	+	+	+	+	+
Pur	Purkinje cell layer of the cerebellar cortex	–	+	+	+	+	+
Type 3a (peak expression is moderate, and seen in the second week of age)							
Rt	Thalamic reticular nucleus	+	+	++	++	+	+
Type 3b (peak expression is weak, and seen in the second week of age)							
MoCV	Layer V in the motor cortex	–	–	+	+	–	–
SoCV	Layer V in the somatosensory cortex	–	–	+	+	–	–
AuCV	Layer V in the auditory cortex	–	–	+	+	–	–
ViCV	Layer V in the visual cortex	–	–	+	+	–	–
CgV	Layer V in the cingulate cortex	–	+	+	+	–	–
RSCII	Layer II in the retrosplenial cortex	–	–	+	+	–	–
RSCV	Layer V in the retrosplenial cortex	+	+	+	+	–	–

+++, strong expression; ++, moderate expression; +, weak expression; –, undetectable expression.
P0, P4, P7, P14, P28, and P8W indicate postnatal days 0, 4, 7, 14, and 28, and postnatal week 8, respectively.
Abbreviations of the nomenclature are described in the far left column.

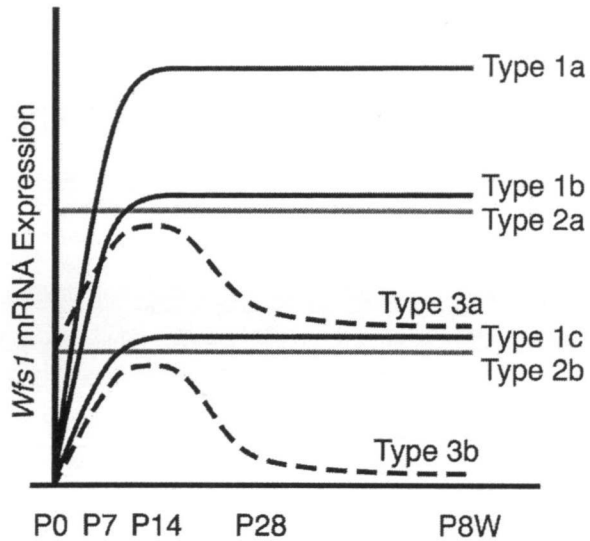

Fig. 1. A graph showing a general impression of postnatal changes in the strength of *Wfs1* mRNA expression in each structure of the mouse brain. Black-solid, shaded-solid, and black-dashed lines indicate types 1, 2, and 3 patterns, respectively. Upper part of the graph represents stronger *Wfs1* mRNA expression. P0, P7, P14, P28, and P8W show postnatal days 0, 7, 14, and 28, and postnatal week 8, respectively. Note that the patterns are categorized into three types. In addition, each type is classified into two or three subtypes (e.g. 1a, 1b, and 1c) according to the maximum strength of *Wfs1* mRNA expression during postnatal development.

impression of the changes is provided in Fig. 1, which shows a graph, depicting patterns of change in the strength of *Wfs1* mRNA expression from birth to early adulthood. As shown in Fig. 1, the patterns were classified into three types (1, 2, and 3) according to the strength of *Wfs1* mRNA expression at different developmental stages. In the type 1 pattern, *Wfs1* mRNA signals were weak or absent on delivery day (P0), progressively increased from P0 to postnatal day 14 (P14), and were of a relatively stable strength from P14 to early adulthood (postnatal week 8; P8W). In addition, type 1 was categorized into three subtypes (1a, 1b, and 1c) according to the strength of *Wfs1* mRNA expression from P14 to early adulthood (P8W). In type 1a, strong *Wfs1* mRNA signals were seen from P14 to early adulthood (P8W). This pattern was observed in the CA1 field of the hippocampus (CA1), the medial entorhinal area (MEA), the lateral entorhinal area (LEA), and in the parasubiculum (PaS) (Figs. 1 and 2; Table 1). In type 1b, moderate *Wfs1* mRNA signals were seen from P14 to early adulthood (P8W). This pattern was observed in layer II of the motor (MoCII) and cingulate (CgII) cortices, the piriform cortex (Pir), the lateral septal nucleus (LS), nucleus accumbens (Acb), the mesencephalic trigeminal nucleus (Me5), the medial subdivision of the facial nucleus (7NM), and in nucleus ambiguus (Amb) (Figs. 1, 3, 4G–L; Table 1). In type 1c, weak *Wfs1* mRNA signals were seen from P14 to early adulthood (P8W). This pattern was observed in layer II of the somatosensory (SoCII), auditory (AuCII) and visual (ViCII) cortices, and in the superior colliculus (SC) (Fig. 1; Table 1).

In the type 2 pattern, *Wfs1* mRNA signals were of a relatively constant strength from P0 to early adulthood (P8W). Like type 1,

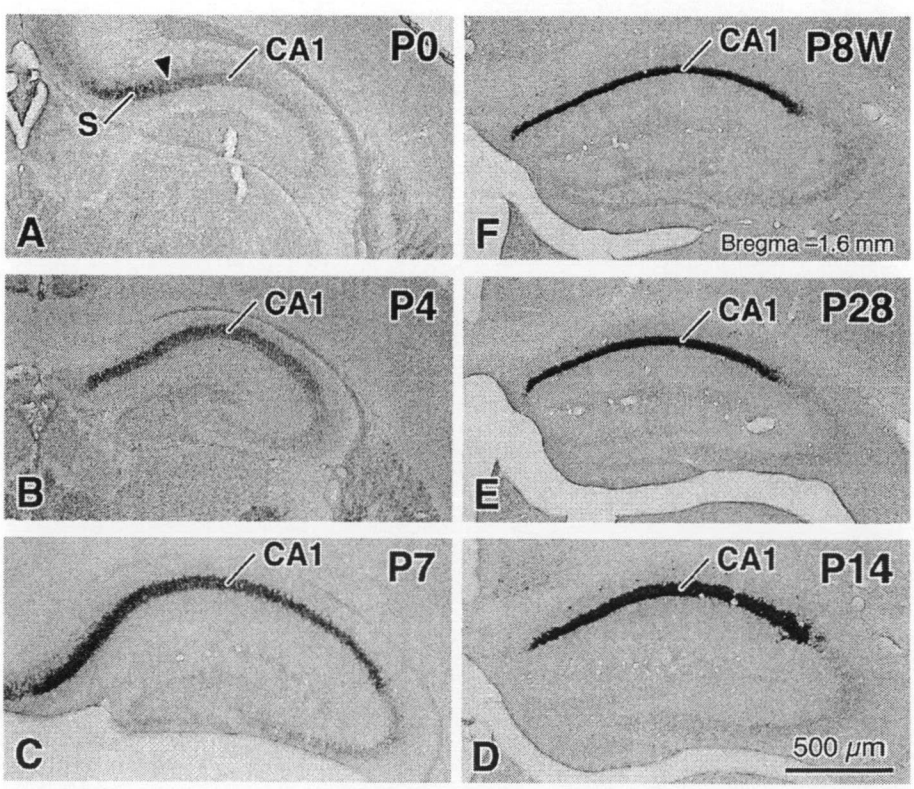

Fig. 2. Type 1a pattern of *Wfs1* mRNA signals in the mouse brain during postnatal development. (A–F) Changes in *Wfs1* mRNA signals in the CA1 field of the hippocampus (CA1) during postnatal development. The day of birth is regarded as postnatal day 0 (P0). P4, P7, P14, P28, and P8W indicate postnatal days 4, 7, 14, and 28, and postnatal week 8, respectively. Brain sections of P0, P4, P7, P14, P28, and of P8W mice are shown in panels (A), (B), (C), (D), (E), and (F), respectively. The arrowhead in (A) shows the border between the subiculum (S) and the CA1 field. The bregma level of a P8W-mouse section is represented at the lower right in (F). Scale bar = 500 μm in (D) for (A–C) and for (E and F). (G–L) Changes in *Wfs1* mRNA signals in the parasubiculum (PaS) and the medial entorhinal area (MEA) during postnatal development. Brain sections of P0, P4, P7, P14, P28, and of P8W mice are shown in panels (G), (H), (I), (J), (K), and (L), respectively. Arrowheads in (H–L) show the boundary between the PaS and the MEA. The bregma level of a P8W-mouse section is represented at the lower right in (L). Note that *Wfs1* mRNA signals in the type 1a pattern are weak or absent on P0, progressively increase from P0 to P14, are strong on P14, and are of a relatively stable strength from P14 to P8W. LEA, lateral entorhinal area. Scale bar = 500 μm in (J) for (G–I) and for (K and L).

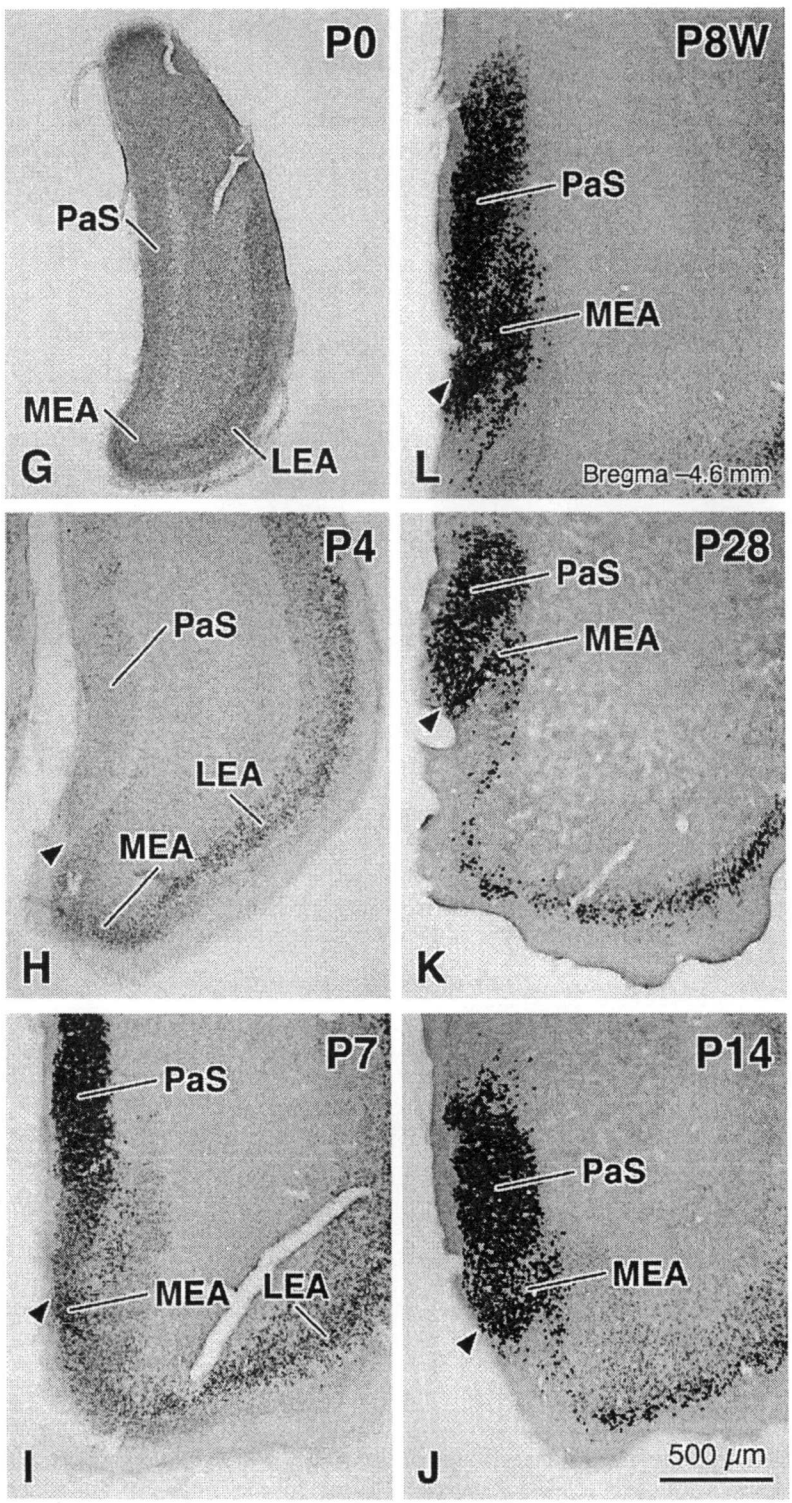

Fig. 2. (*Continued*).

type 2 was categorized into two subtypes (2a and 2b) according to the strength of *Wfs1* mRNA expression from P0 to early adulthood (P8W). In type 2a, moderate *Wfs1* mRNA signals were invariably seen. This pattern was mainly observed in the limbic structures, and in the brainstem motor nuclei. It was found in the subiculum (S), the olfactory tuberculum (Tu), the lateral bed nucleus of the stria terminalis (BSTL), the interstitial nucleus of the posterior limb of the anterior commissure (IPAC), the central amygdaloid nucleus (Ce), the caudal part of the caudate putamen (CPu), the motor nucleus of the trigeminal nerve (Mo5), the lateral subdivision of the facial nucleus (7NL), and in the hypoglossal nucleus (12N) (Figs. 1 and 4; Table 1). As described above, in the facial nucleus,

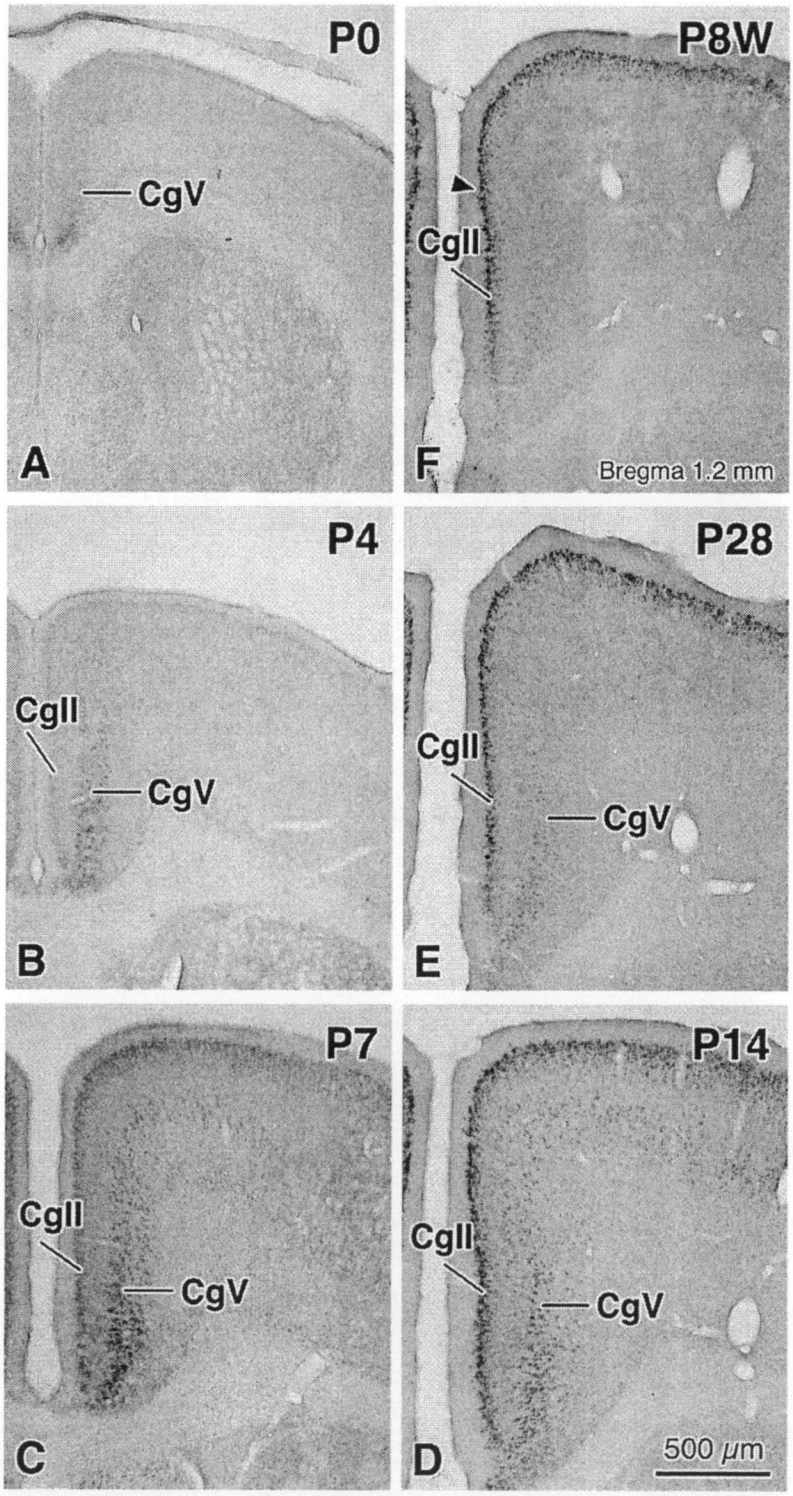

Fig. 3. Type 1b pattern of *Wfs1* mRNA signals in the mouse brain during postnatal development. (A–F) Changes in *Wfs1* mRNA signals in layer II of the cingulate cortex (CgII) during postnatal development. The day of birth is regarded as postnatal day 0 (P0). P4, P7, P14, P28, and P8W indicate postnatal days 4, 7, 14, and 28, and postnatal week 8, respectively. Brain sections of P0, P4, P7, P14, P28, and of P8W mice are shown in panels (A), (B), (C), (D), (E), and (F), respectively. The arrowhead in (F) shows the border between the cingulate cortex and the motor cortex. The bregma level of a P8W-mouse section is represented at the lower right in (F). A type 3b pattern is seen in layer V of the cingulate cortex (CgV). Scale bar = 500 μm in (D) for (A–C) and for (E and F). (G–L) Changes in *Wfs1* mRNA signals in the lateral septal nucleus (LS) during postnatal development. Brain sections of P0, P4, P7, P14, P28, and of P8W mice are shown in panels (G), (H), (I), (J), (K), and (L), respectively. The bregma level of a P8W-mouse section is represented at the lower right in (L). Note that *Wfs1* mRNA signals in the type 1b pattern are weak or absent on P0, progressively increase from P0 to P14, are moderate on P14, and are of a relatively stable strength from P14 to P8W. CPu, caudate putamen. Scale bar = 500 μm in (J) for (G–I) and for (K and L).

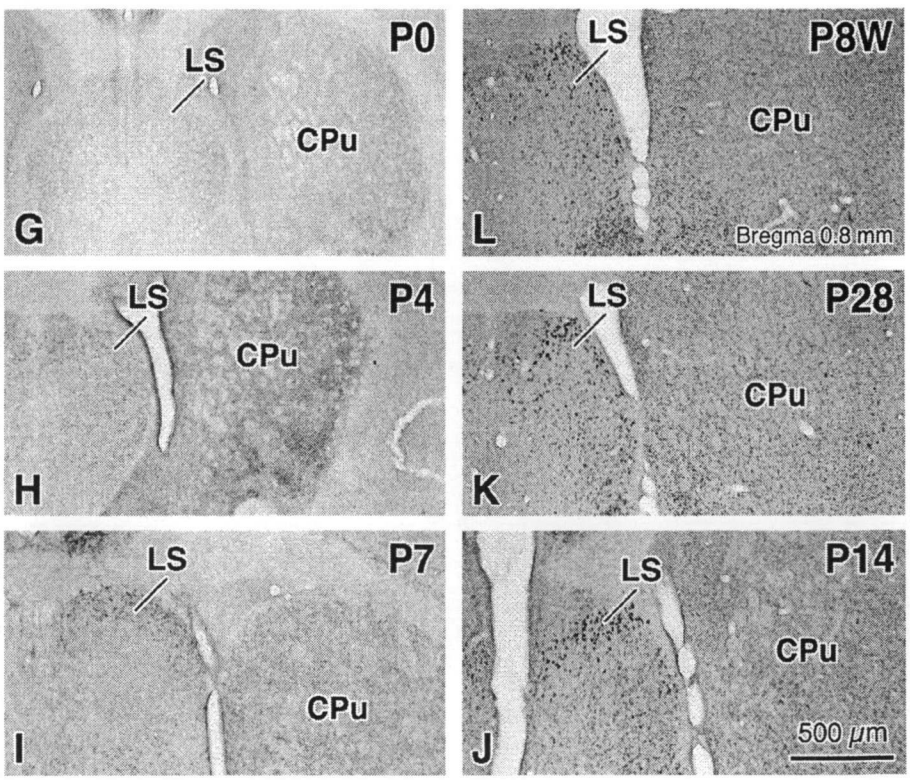

Fig. 3. (*Continued*).

the type 2a pattern was seen in the lateral subdivision (7NL), whereas the type 1b pattern was observed in the medial subdivision (7NM) (Fig. 4G–L; Table 1). In type 2b, weak *Wfs1* mRNA signals were constantly seen at each of the postnatal stages. This pattern was observed in the main olfactory bulb (MOB), the accessory olfactory bulb (AOB), the supraoptic nucleus (SO), the magnocellular part of the paraventricular hypothalamic nucleus (PVNm), the inferior colliculus (IC), nucleus coeruleus (LC), the dorsal raphe nucleus, the median raphe nucleus, the cochlear nucleus (Co), the brainstem reticular formation, and in the Purkinje cell layer of the cerebellar cortex (Figs. 1 and 5A–F; Table 1).

In the type 3 pattern, *Wfs1* mRNA signals peaked from P7 to P14. Type 3 was also categorized into two subtypes (3a and 3b) according to the strength of *Wfs1* mRNA expression at its peak. In type 3a, moderate *Wfs1* mRNA signals were seen from P7 to P14, while weak signals were observed at both P0–P4 and P28–early adulthood (P8W). This pattern was observed in the thalamic reticular nucleus (Rt) (Figs. 1, 5G–L; Table 1). In type 3b, weak *Wfs1* mRNA signals were seen from P7 to P14. This pattern was observed in layer V of the cerebral cortices: the motor (MoCV), somatosensory (SoCV), auditory (AuCV), visual (ViCV), cingulate (CgV), and retrosplenial (RSCV) cortices (Figs. 1, 3A–F; Table 1). It was also seen in layer II of the retrosplenial cortex (RSCII) (Table 1).

3.2. Strong Wfs1 mRNA expression in the CA1 field, parasubiculum (PaS), and entorhinal cortex in early adulthood

As described in the preceding section, the most intense *Wfs1* mRNA signals were observed in the CA1 field, the PaS, and in the entorhinal cortex (MEA and LEA) from P14 to early adulthood (P8W). To examine cell-specific *Wfs1* mRNA expression, we made a detailed analysis of the distribution of *Wfs1* mRNA signals in these cortical areas of the young-adult mouse (P8W) as a preliminary account of a future analysis of the entire mouse brain structure. Because definitions of areal demarcation and laminar classification are necessary for the interpretation of the experimental results, we will briefly describe our criteria for determining the border of the cortical area and those of the cortical layer before describing the distribution of *Wfs1* mRNA signals. In addition, a description of the pertinent cytoarchitectonic features of each cortical area is accompanied by a description of the distribution of *Wfs1* mRNA signals. To represent the distribution of *Wfs1* mRNA signals, we show side by side the features of the distribution and Nissl-stained sections that correspond to the distribution in the figures.

3.2.1. CA1 field

3.2.1.1. Cytoarchitecture. Areal demarcation was based on Witter and Amaral (2004). According to the size of pyramidal cells in the hippocampus proper, the CA1 field was defined as a small-celled distal (closer to the subiculum) region, while the CA2 and CA3 fields were characterized as large-celled proximal (closer to the dentate gyrus) region. In the CA3 field, small Nissl-stained cells were scattered above the pyramidal cell layer (arrows in Fig. 6B), however a few of these cells were seen in the CA1 and CA2 fields (Fig. 6B).

3.2.1.2. Wfs1 mRNA signals. Wfs1 mRNA signals were observed in the pyramidal cell layer. These signals were confined to the CA1 field. Strong signals were observed in the rostro-medial (septal) part of the CA1 field (Fig. 6A), while weak-to-moderate signals were seen in the caudo-lateral (temporal) part (data not shown). In the rostral part of the CA1 field, there was a tendency for *Wfs1* mRNA signals to be stronger in the medial part than in the lateral part (Fig. 6A). In addition to the pyramidal cell layer, weakly-to-moderately *Wfs1* mRNA-hybridized neurons were seen in strata radiatum and oriens (arrows in Fig. 6A and C).

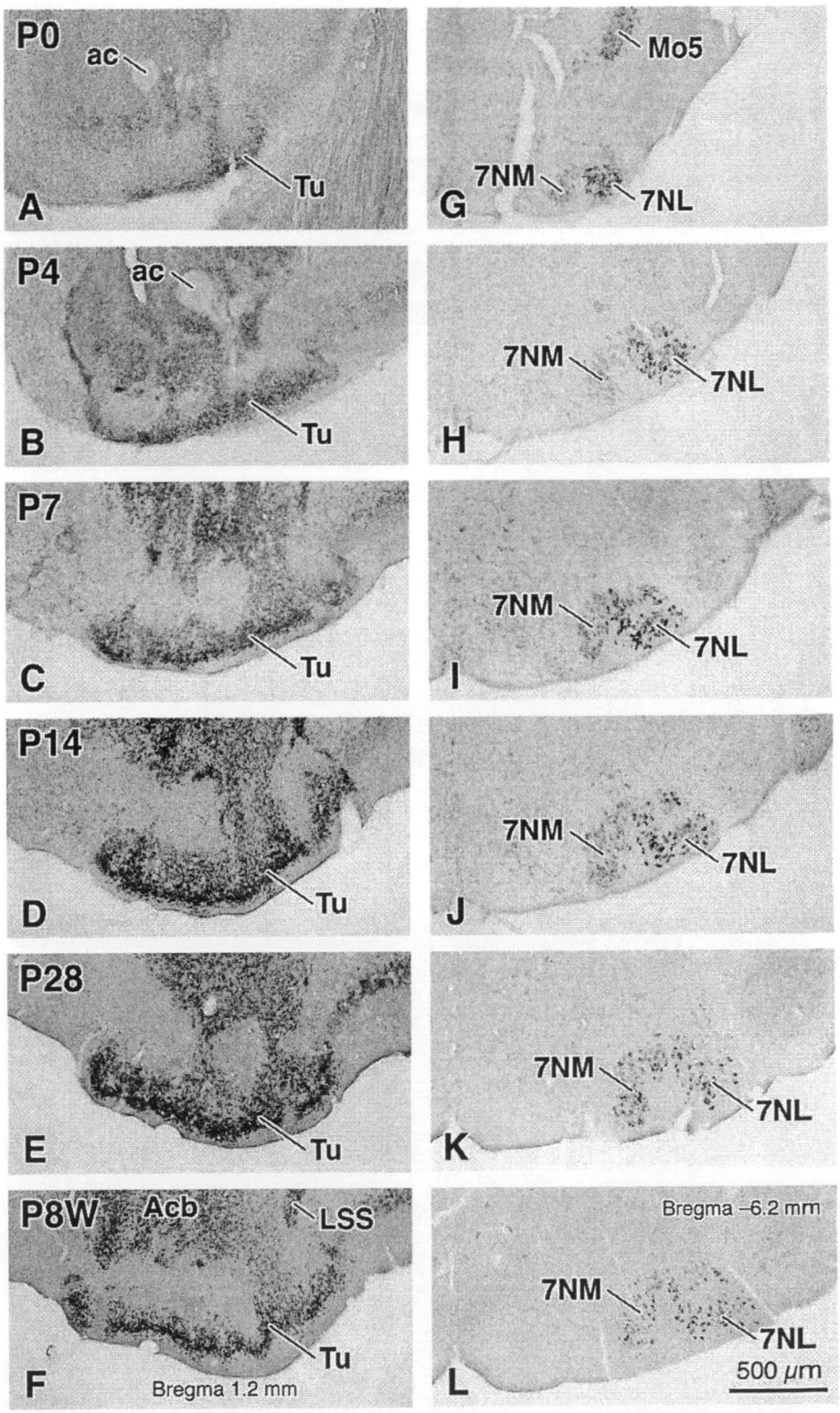

Fig. 4. Type 2a pattern of *Wfs1* mRNA signals in the mouse brain during postnatal development. (A–F) Changes in *Wfs1* mRNA signals in the olfactory tuberculum (Tu) during postnatal development. The day of birth is regarded as postnatal day 0 (P0). P4, P7, P14, P28, and P8W indicate postnatal days 4, 7, 14, and 28, and postnatal week 8, respectively. Brain sections of P0, P4, P7, P14, P28, and of P8W mice are shown in panels (A), (B), (C), (D), (E), and (F), respectively. The bregma level of a P8W-mouse section is represented at the lower middle in (F). (G–L) Changes in *Wfs1* mRNA signals in the facial nucleus during postnatal development. Brain sections of P0, P4, P7, P14, P28, and of P8W mice are shown in panels (G), (H), (I), (J), (K), and (L), respectively. The bregma level of a P8W-mouse section is represented at the upper right in (L). Note that *Wfs1* mRNA signals in the type 2a pattern are moderate, and of a relatively stable strength from P0 to P8W. Additionally, in the facial nucleus, the pattern of *Wfs1* mRNA signals during postnatal development is not homogeneous. In the lateral subdivision of the facial nucleus (7NL), the pattern is type 2a, whereas in the medial subdivision (7NM), it is type 1b. Upper and right sides of each panel are dorsal and lateral sides of each brain section, respectively. ac, anterior commissure; Acb, nucleus accumbens, LSS, lateral stripe of the striatum; Mo5, motor nucleus of the trigeminal nerve. Scale bar = 500 μm in (L) for (A–K).

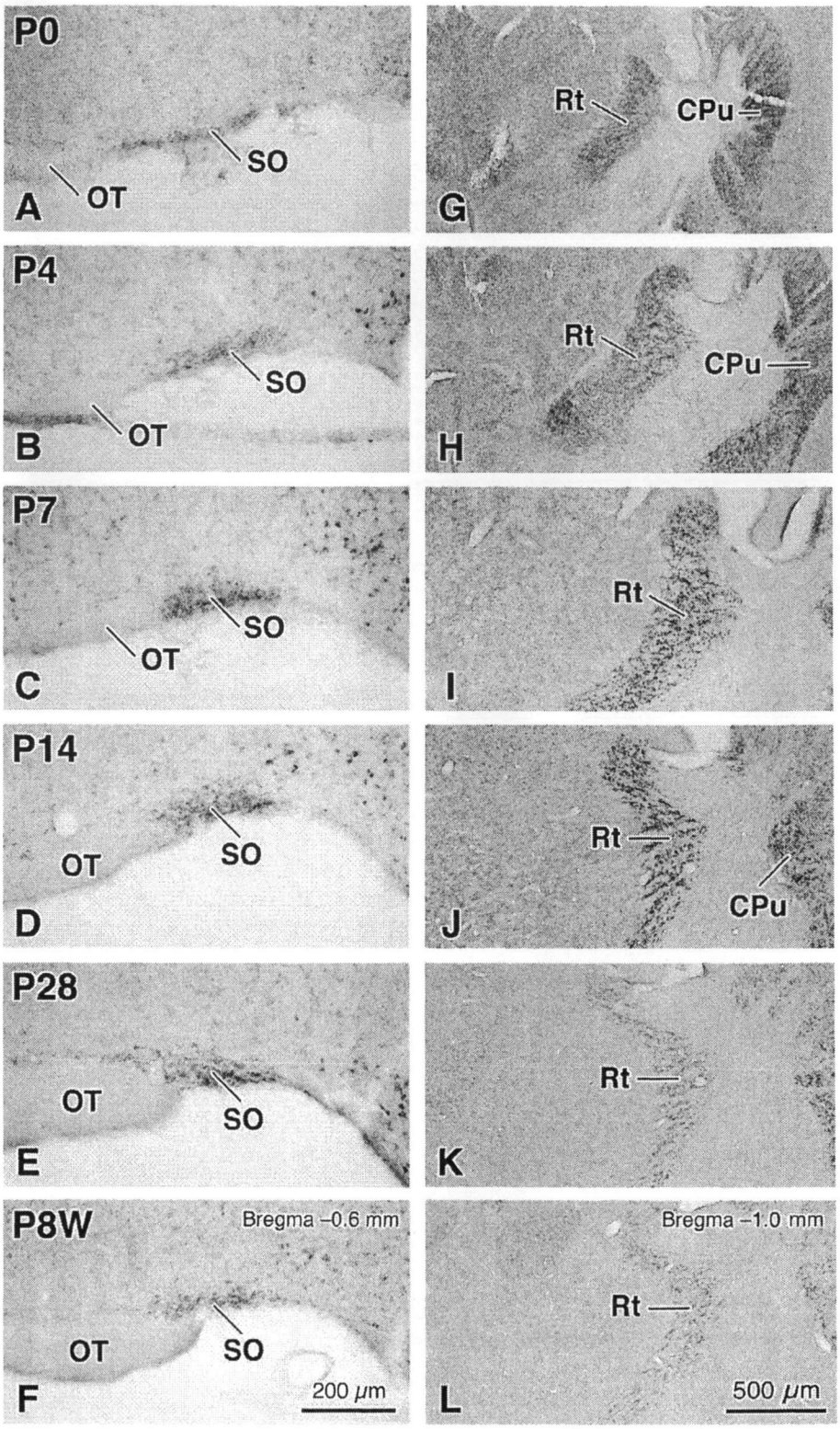

Fig. 5. Type 2b (A–F) and type 3a (G–L) patterns of *Wfs1* mRNA signals in the mouse brain during postnatal development. (A–F) Changes in *Wfs1* mRNA signals in the supraoptic nucleus (SO) during postnatal development. The day of birth is regarded as postnatal day 0 (P0). P4, P7, P14, P28, and P8W indicate postnatal days 4, 7, 14, and 28, and postnatal week 8, respectively. Brain sections of P0, P4, P7, P14, P28, and of P8W mice are shown in panels (A), (B), (C), (D), (E), and (F), respectively. The bregma level of a P8W-mouse section is represented at the upper right in (F). Note that *Wfs1* mRNA signals in the type 2b pattern are weak, and of a relatively stable strength from P0 to P8W. (G–L) Changes in *Wfs1* mRNA signals in the thalamic reticular nucleus (Rt) during postnatal development. Brain sections of P0, P4, P7, P14, P28, and of P8W mice are shown in panels (G), (H), (I), (J), (K), and (L), respectively. The bregma level of a P8W-mouse section is represented at the upper right in (L). Note that *Wfs1* mRNA signals in the type 3a pattern peak from P7 to P14 and show moderate strength at the peak. Upper and right sides of each panel are dorsal and lateral sides of each brain section, respectively. CPu, caudate putamen; OT, optic tract. Scale bar = 200 μm in (F) for (A–E), 500 μm in (L) for (G–K).

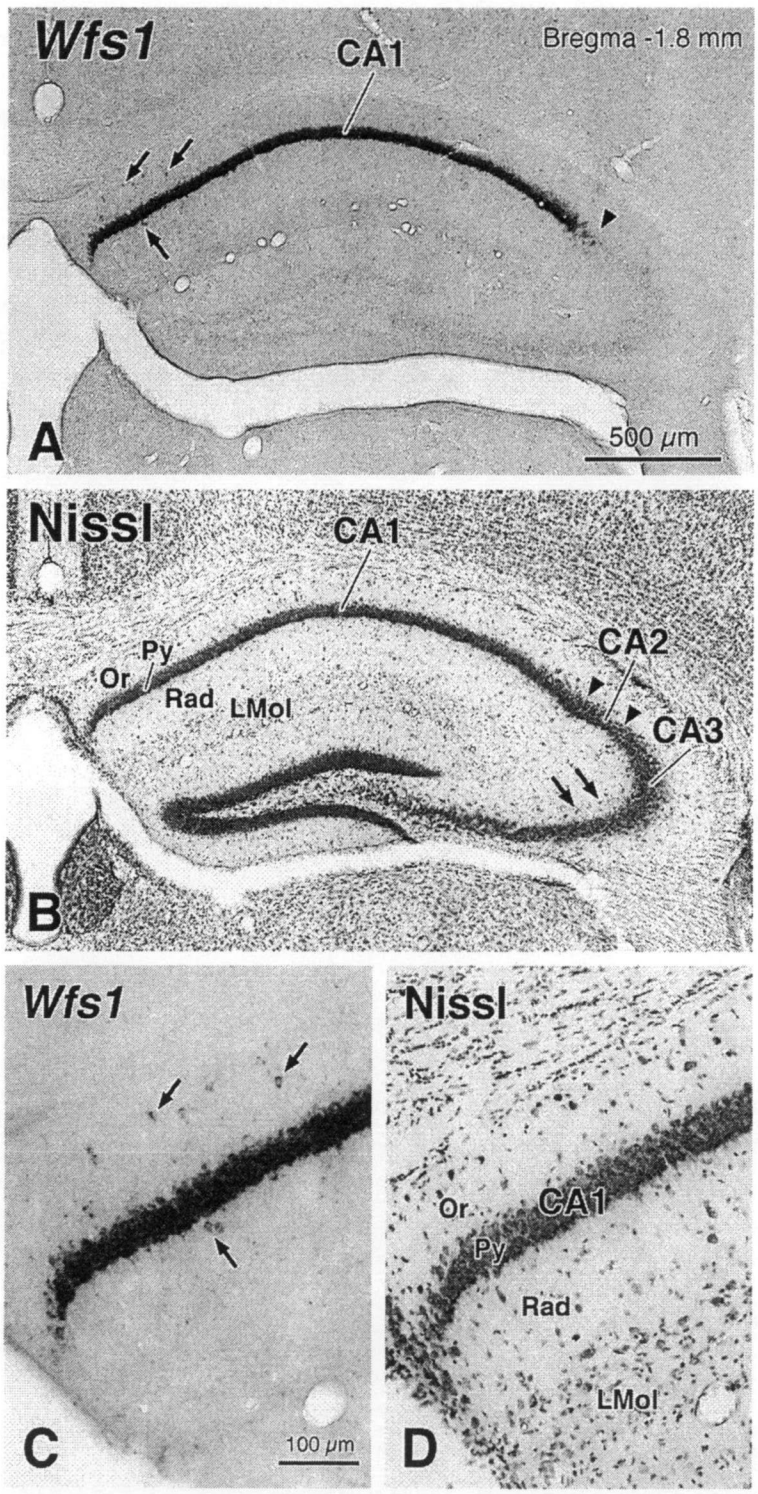

Fig. 6. *Wfs1* mRNA signals in the rostral part (Bregma = −1.8 mm) of the hippocampal formation in the young-adult mouse (postnatal week 8). (A and B) Mouse *Wfs1* mRNA signals (*Wfs1*, A), and cytoarchitecture (Nissl, B) in adjacent sections of the hippocampal formation hybridized with anti-sense cRNA probes of the mouse *Wfs1* 3′-terminus, and Nissl-stained with cresyl violet, respectively. Arrowheads indicate borders between each hippocampal field. Arrows in (A), and those in (B) show *Wfs1* mRNA-hybridized neurons in strata radiatum and oriens of the CA1 field, and small Nissl-stained cells scattered above the pyramidal cell layer of the CA3 field, respectively. (C and D) Higher magnification photomicrographs of mouse *Wfs1* mRNA signals (*Wfs1*, C) in the same section as in panel (A) and of cytoarchitecture (Nissl, D) in the same section as in panel (B). Arrows in (C) show the identical set of *Wfs1* mRNA-hybridized neurons pointed to by arrows in (A). Note that strong *Wfs1* mRNA signals are almost exclusively observed in the pyramidal cell layer of the CA1 field. In addition, *Wfs1* mRNA-hybridized neurons (arrows in A and C) are seen in strata oriens and radiatum of the CA1 field. CA1, CA1 field of the hippocampus; CA2, CA2 field of the hippocampus; CA3, CA3 field of the hippocampus; LMol, stratum lacunosum-moleculare; Or, stratum oriens; Py, pyramidal cell layer; Rad, stratum radiatum. Scale bars = 500 μm in (A) for (B), 100 μm in (C) for (D).

3.2.2. PaS

3.2.2.1. Cytoarchitecture. Areal demarcation and the laminar classification were based on Witter and Amaral (2004). From the cytoarchitectonic aspect, the PaS (Brodmann's area 49) is a multilayered structure in which there are more than three cortical layers. The layers of the PaS are subdivided into external and internal laminae, separated by a cell-free lamina (layer IV). The external lamina is composed of the molecular layer (layer I) and cell layers II and III, and the internal lamina, cell layers V and VI. Layers II and III comprise large, rather densely packed, lightly stained cells. There is no clear boundary between layers II and III of the external lamina. Layers V and VI consist of small, rather densely packed, moderately stained cells (Fig. 7B and D).

3.2.2.2. Wfs1 mRNA signals. Strong *Wfs1* mRNA signals were observed in cell layers II and III (the external lamina except for layer I). In the deep part of the external lamina, weak-to-moderate signals were also seen deeper down (Fig. 7).

3.2.3. Entorhinal cortex

3.2.3.1. Cytoarchitecture. Areal demarcation and the laminar classification were based on Insausti et al. (1997) and on Witter and

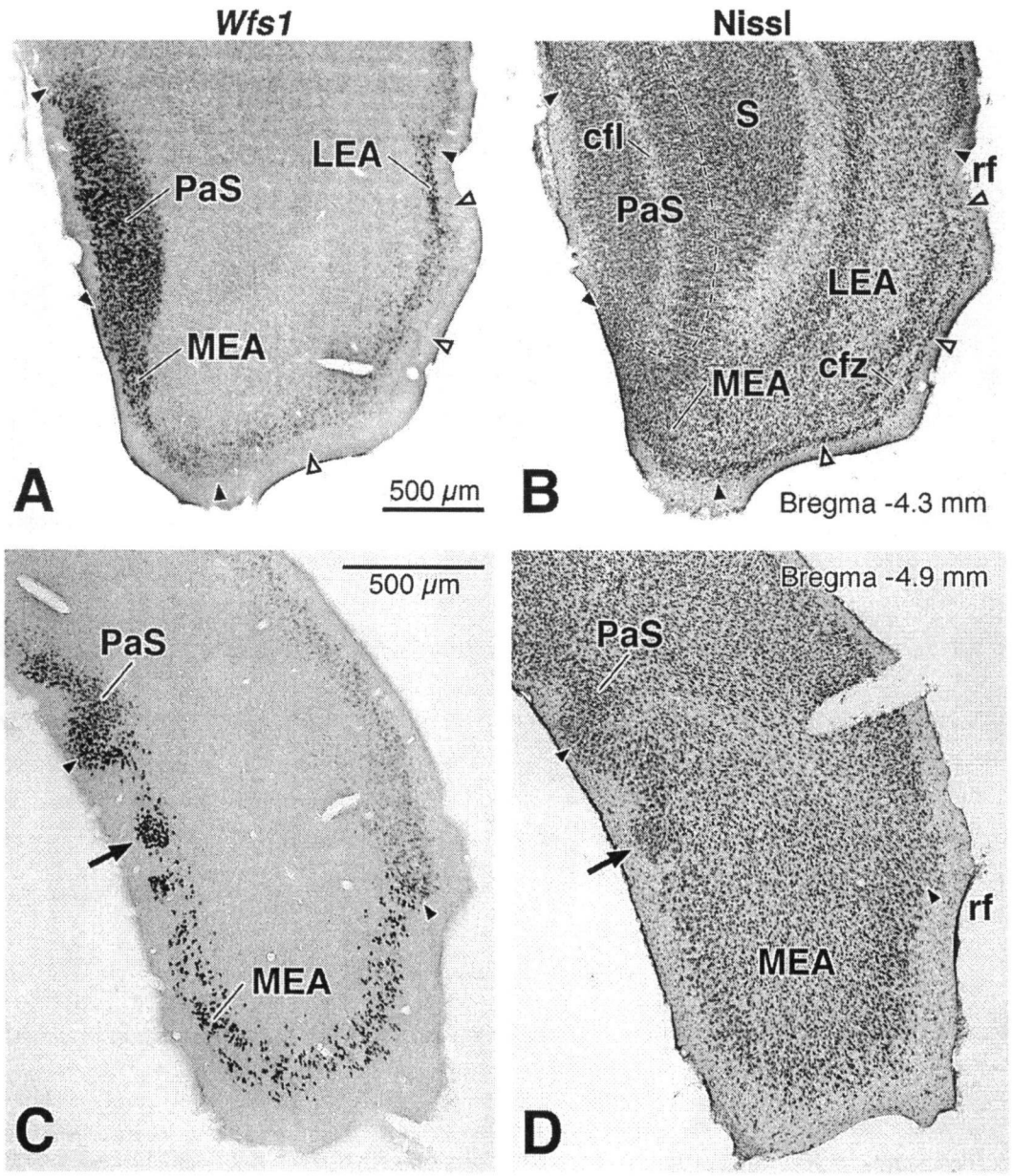

Fig. 7. *Wfs1* mRNA signals in the parasubiculum (PaS) and entorhinal cortex of the young-adult mouse (postnatal week 8). (A and B) Mouse *Wfs1* mRNA signals (*Wfs1*, A), and cytoarchitecture (Nissl, B) in adjacent sections of the rostral part (Bregma = −4.3 mm) hybridized with anti-sense cRNA probes of the mouse *Wfs1* 3′-terminus, and Nissl-stained with cresyl violet, respectively. The dashed line in (B) shows the border of the PaS. (C and D) Mouse *Wfs1* mRNA signals (*Wfs1*, C), and cytoarchitecture (Nissl, D) in adjacent sections of the caudal part (Bregma = −4.9 mm). Solid and open arrowheads indicate borders between each cortical area and the superficial boundary of layer II in the lateral entorhinal area (LEA), respectively. Arrows show an islet of cells in layer II of the medial entorhinal area (MEA). Note that strong *Wfs1* mRNA signals are observed in the PaS, MEA, and LEA. cfl, cell-free lamina; cfz, cell-free zone; rf, rhinal fissure; S, subiculum. Scale bars = 500 μm in (A) for (B), in (C) for (D).

Amaral (2004). In this study, the entorhinal cortex is subdivided into two areas, the MEA and the LEA. In the MEA, cells in layer II are primarily large-to-medium-sized, moderately packed, and moderately stained, while those in layer III are small-to-medium-sized and loosely packed (Fig. 7B and D). In the caudo-medial part of layer II, an islet of cells (arrow in Fig. 7D) was observed. Cells in the islet were medium-sized, rather densely packed, and lightly stained (Fig. 7D). In the rostro-medial part, which abuts the PaS, layer I is very thin and layers II and III contain densely packed cells that are small-to-medium-sized, and moderately stained (Fig. 7B).

In the LEA, layer II is separated from layer III by a narrow cell-free zone in much of the rostral part. Cells in layer II are very densely packed, while those in layer III are moderately or loosely packed. Layer III is thick and subdivided into a narrow moderately packed outer zone and a loosely packed inner zone. Since layer IV is very poorly developed or absent, layer V usually abuts layer III. Cells in layer V tend to be larger and more darkly stained than those in layer III (Fig. 7B).

3.2.3.2. Wfs1 mRNA signals. In the caudal part of the MEA, strong *Wfs1* mRNA signals were observed in layer II. These signals were almost confined to this layer (Fig. 7C and D). In layer II of the caudo-medial part, islets of strongly *Wfs1* mRNA-hybridized cells were seen (arrow in Fig. 7C). One of these islets corresponded to an islet of Nissl-stained cells (arrow in Fig. 7D). Strongly *Wfs1* mRNA-hybridized cells were densely packed in the islets, while those were scattered around the islets (Fig. 7C). In the rostro-medial part of the MEA, strongly-to-moderately *Wfs1* mRNA-hybridized cells were seen in layers II and III. In the rostro-lateral part of the MEA, weak *Wfs1* mRNA signals were detected in layer II (Fig. 7A and B).

In the LEA, strong *Wfs1* mRNA signals were observed in the outer zone of layer III. The distribution of these signals was confined to around the rhinal fissure (Fig. 7A and B). In the other part of the LEA, weak-to-moderate signals were seen in layer III deeper down. Different from the other multi-layered cortical areas, a very small number of *Wfs1* mRNA signals was detected in layer II (Fig. 7A and B).

4. Discussion

In the present study, we determined the patterns of change in the strength of *Wfs1* mRNA signals in each of the mouse brain structures from birth to early adulthood (P8W). There were three patterns. In type 1, signals were weak or absent in neonates but strong or moderate in young adults. This pattern was observed in the CA1 field, the PaS, and in the entorhinal cortex (MEA and LEA). In type 2, signals were of a relatively constant strength during development. This pattern was seen in limbic structures (e.g. S (subiculum) and Ce (central amygdaloid nucleus)) and brainstem nuclei (e.g. facial and chochlear nuclei). In type 3, signals peaked in the second week of age. This pattern was observed in the Rt (thalamic reticular nucleus). The present study also demonstrated layer-specific localization of *Wfs1* mRNA signals in the CA1 field, the PaS, and in the entorhinal cortex where strong signals were seen from P14 to early adulthood (P8W).

4.1. Comparison with previous findings

Our findings on *Wfs1* mRNA expression in the brain of young-adult mice were primarily compatible with previous studies in the mouse (Kato et al., 2008; Kawano et al., 2008; Luuk et al., 2008) and the rat (Takeda et al., 2001). In these studies, *Wfs1* expression was described in the cerebral cortex, the basal ganglia, the hypothalamus, the brain stem motor and sensory nuclei, the reticular formation, and in the cerebellar cortex, as well as in the CA1 field and in the amygdala. The present study showed that *Wfs1* mRNA signals were observed in these structures of the young-adult mouse. The findings indicate that *Wfs1* mRNA expression in these structures (present study) is similar to Wfs1 protein expression (Kato et al., 2008; Luuk et al., 2008), and is similar between the mouse (present study) and the rat (Takeda et al., 2001) in early adulthood.

4.2. Patterns of change in Wfs1 mRNA expression

In the following, we discuss each type of the patterns of change in the strength of *Wfs1* mRNA signals systematically.

4.2.1. Type 1 pattern of change

4.2.1.1. Type 1a. Type 1a pattern was observed in the limbic cortex: the CA1 field, PaS, MEA, and LEA. The CA1 field is a part of the hippocampus proper, and the PaS, MEA, and LEA are parts of the parahippocampal cortical areas (Witter and Amaral, 2004). Detailed discussions about these structures are described separately in Section 4.3.

4.2.1.2. Type 1b. Type 1b pattern was observed in the motor, limbic, and olfactory cortices (MoCII, CgII, and Pir), basal nuclei that are parts of the limbic system (LS, and Acb), and in the sensory and motor brainstem nuclei (Me5, 7MN, and Amb). The cingulate cortex is one of the largest components of the limbic system and is characterized by diffuse projections from the anteromedial thalamic nucleus (Palomero-Gallagher and Zilles, 2004). It is involved in motivational aspects of learning tasks (Gabriel et al., 1980) and contributes to motor functions via numerous efferents to subcortical motor systems (Palomero-Gallagher and Zilles, 2004). The Pir (piriform cortex) is a part of the primary olfactory cortex, since the Pir receives direct projections from the MOB (main olfactory bulb) (Shipley et al., 2004). The LS (lateral septal nucleus) is characterized by massive glutamatergic afferents from the hippocampus proper and the subiculum, and by massive bidirectional connections with the rostral brainstem, especially with the hypothalamus and the ventral midbrain. The LS contributes to emotional behaviors (Risold, 2004). The Acb (nucleus accumbens) is a limbic part of the striatum. This nucleus receives extensive inputs from limbic structures, such as the hippocampus and amygdala, as well as from the prefrontal areas subserving limbic and autonomic functions, i.e. orbital, infralimbic, prelimbic, and agranular insular cortices. The Acb reciprocates its dopaminergic input, and in addition, innervates most of the dopaminergic neurons projecting to the associative and motor structures (Joel and Weiner, 2000). The Me5 (mesencephalic trigeminal nucleus) is one of the sensory relay nuclei, and plays a role in proprioception during mastication and the integration of jaw movements (Waite, 2004). The Amb (nucleus ambiguus) is one of the branchial motor nuclei in the brainstem, and innervates the striated muscles of the pharynx, esophagus, and larynx (Loewy and Spyer, 1990; Saper, 2000). It is possible that the Me5 and the Amb contribute to feeding. Further details concerning the 7NM are described separately in Section 4.4.

4.2.1.3. Type 1c. Type 1c pattern was observed in layer II of the sensory cortical areas except for the olfactory area (SoCII, AuCII, and ViCII), and in the SC. There are some striking similarities between the sensory cortical areas and the SC: both structures have layered architecture, the both structures receive few olfactory inputs, and the both structures contribute to process sensory information including visual, somatosensory, and auditory modalities (Sefton et al., 2004).

4.2.2. Type 2 pattern of change

4.2.2.1. Type 2a. Type 2a pattern was observed in the limbic structures (S, Tu, BSTL, IPAC, and Ce), the caudal part of the CPu, and

in the oromotor nuclei relevant to feeding (Mo5, 7NL, and 12N). The S (subiculum) is a part of the hippocampal formation and is the major origin of the fornix (Witter and Amaral, 2004). The Tu (olfactory tuberculum) is referred to as a part of the primary olfactory cortex, since the Tu receives direct projections from the MOB. In addition, the Tu is regarded as a part of the ventral striatum, the limbic part of the striatum (Shipley et al., 2004). The BSTL (lateral bed nucleus of the stria terminalis) and the IPAC (interstitial nucleus of the posterior limb of the anterior commissure) are parts of the central division of the extended amygdala. This means that characteristics of the BSTL and the IPAC are similar to those of the Ce (central amygdaloid nucleus): the BSTL and the IPAC maintain close structural, cytochemical, and hodological relationships with the Ce (de Olmos et al., 2004). The Ce is believed to be an important output region of the amygdala, at least for the expression of innate emotional responses and associated physiological responses. The expression of these responses involves connections from the medial subdivision of the Ce to brainstem areas that control specific behaviors and physiological responses (LeDoux, 2007).

In general, the CPu (dorsal striatum or neostriatum) is subdivided into medial and lateral from the anato-functional aspect of view. The lateral CPu is regarded as motor striatum, and the medial CPu is regarded as associative striatum (Joel and Weiner, 2000). In addition, anatomical differences between the rostral and caudal CPu were also reported in the rodent striatum. The distribution of μ (mu) opiate receptors demonstrated that spatial organization of patch and matrix compartments in the rat striatum was different between rostral and caudal parts: patches were numerous and of large size in the rostral part, while they were rare and of small size in the caudal part (Desban et al., 1993). As for corticostriatal projections to the matrix in the rat striatum, patterns of axonal arborization were different between the rostral and caudal parts: the extended axonal arborizations were primarily confined to the rostral part, conversely, the focal axonal arborizations were observed most obvious in the caudal part (Kincaid and Wilson, 1996). Since there are anatomical differences between the rostral and caudal parts of the rodent CPu, it is possible to accept that the type 2a pattern of change in the mouse CPu was confined to the caudal part. Further details concerning the oromotor nuclei (Mo5, 7NL, and 12N) are described separately in Section 4.4.

4.2.2.2. Type 2b. Interestingly, brain structures potentially relevant to the clinical symptoms of Wolfram syndrome showed the type 2b pattern of change. Detailed discussions concerning the clinical symptoms are described separately in Sections 4.5–4.7. In addition, brain structures, where atrophic changes were observed in Wolfram syndrome patients, also represented the type 2b pattern. For example, the main and accessory olfactory bulbs (MOB and AOB) showed the type 2b pattern in the mouse. In Wolfram syndrome patients, atrophic changes were observed in the olfactory bulb and tracts (Genís et al., 1997; Shannon et al., 1999). Further details concerning the atrophic changes are given in Section 4.8.

4.2.3. Type 3 pattern of change

4.2.3.1. Type 3a. The Rt (thalamic reticular nucleus), which showed the type 3a pattern, forms a thin neuronal sheet at the rostral, dorsolateral, lateral, and ventrolateral edges of the dorsal thalamus (Groenewegen and Witter, 2004). Groenewegen and Witter (2004) noted that the Rt was strategically "placed" between the dorsal thalamus and the cerebral hemisphere: all incoming and outgoing fibers of the thalamus have to pass through the Rt, and most of the giving off collaterals terminates at a restricted part of the Rt. Thalamic reticular neurons are all GABAergic and express parvalbumin (Mitrofanis, 1992). The prevailing interpretation of the functional role of the Rt is that it serves attentional brain mechanisms (e.g., "searchlight hypothesis") (Crick, 1984; Guillery et al., 1998; McAlonan et al., 2000). The Rt is important for the control of the firing mode of thalamocortical projection neurons and, in this way, for the selection of the information that is transferred from the thalamus to the cerebral cortex. The Rt plays an important role as pacemaker during synchronized firing of thalamocortical cells (Groenewegen and Witter, 2004).

4.2.3.2. Type 3b. Type 3b pattern was observed in layer V of the motor (MoCV), sensory (SoCV, AuCV, and ViCV), and of the limbic cortices (CgV, and RSCV) and in layer II of the limbic cortex (RSCII). Interestingly, *Wfs1* mRNA signals in layer II were observed in the motor, sensory, and cingulate cortices in early adulthood, while those were not seen in the retrosplenial cortex. Together with the anterior cingulate cortex, the retrosplenial cortex is involved in the motivational aspects of learning tasks and contributes to motor functions via numerous efferents to subcortical motor systems (Palomero-Gallagher and Zilles, 2004). In addition, many observations support a significant role of the retrosplenial cortex in visuospatial functions. There is massive visual input to the retrosplenial cortex, and major projections from the postsubiculum which is involved in coding for head position in space (Taube et al., 1990; Vogt et al., 2004).

Interestingly, *Wfs1* mRNA expression in layer V of the motor and sensory cortices (type 3b) synchronized with that in the Rt (type 3a). It is not known why the expression in these structures synchronized each other. It should be noted that layer V in the motor and sensory cortices indirectly connect with the Rt by way of the higher order thalamic nuclei (Gabreëls et al., 1998). For example, layer V neurons in the visual cortex send their axons to the lateral posterior nucleus (LP), a higher order nucleus of the visual thalamus (Sefton et al., 2004). Then LP neurons project to the Rt (Groenewegen and Witter, 2004). The indirect connections between layer V and the Rt may provide clues as to the synchronization.

4.3. Strong Wfs1 mRNA signals in the CA1 field, PaS, and entorhinal cortex

4.3.1. CA1 field

The CA1 field is a part of the hippocampus proper. According to an excellent review by Witter and Amaral (2004), the CA1 field has connections with various intrahippocampal, cortical, and subcortical structures. The CA1 field receives intrahippocampal projections from the CA3 field (Schaffer collaterals), and from the CA2 field (Ishizuka et al., 1990). There are only weak associational connections (Tamamaki et al., 1987; Amaral et al., 1991) and weak commissural connections (Van Groen and Wyss, 1990b) in the CA1 field. Cortical inputs to the CA1 field arise from the entorhinal, perirhinal, and postrhinal cortices, which compose the parahippocampal region. The CA1 field receives subcortical projections from the septum, the amygdala, and from the thalamus. It also receives light noradrenergic, serotonergic, and dopaminergic inputs from the brainstem nuclei (Swanson et al., 1987). In addition to the afferent connections, the CA1 field has efferent connections with various intrahippocampal, cortical, and subcortical structures. The major projection arising from the CA1 field is a projection to the adjacent subiculum. With regard to cortical efferents, the CA1 field sends axons back to the parahippocampal region including the entorhinal, perirhinal, and postrhinal cortices. The CA1 field also projects to the retrosplenial, prelimbic, and infralimbic cortices. Subcortical outputs from the CA1 field terminate in the septum, nucleus

accumbens, olfactory structures including the olfactory bulb, the hypothalamus, and in the amygdala (Van Groen and Wyss, 1990b; Witter and Amaral, 2004). Since strong *Wfs1* mRNA signals were observed in the pyramidal layer, the *Wfs1* gene might contribute to these neuronal relays in this layer. However, it is unclear whether *Wfs1* mRNA-hybridized pyramidal cells are involved in all of these neuronal relays. Further studies by using tract-tracing methods are required to clarify the fiber connections of *Wfs1* mRNA-hybridized neurons in the CA1 field.

The principal neuronal cell type of the CA1 field is the pyramidal cell (Witter and Amaral, 2004). Since the pyramidal cell makes up the vast majority of neurons in the pyramidal cell layer (Witter and Amaral, 2004), and since *Wfs1* mRNA signals were seen in most of the cells of this layer (present study), the signals were probably located in pyramidal cells. In addition to the pyramidal cell, there are several types of non-pyramidal cells in strata oriens, radiatum, and lacunosum-moleculare of the CA1 field. The vast majority of these neurons are immunoreactive for GABA (γ-aminobutyric acid; Ribak et al., 1978), and most of these cells are considered to be local circuit neurons (interneurons; Witter and Amaral, 2004). Since *Wfs1* mRNA-hybridized cells were also observed in strata radiatum and oriens of the CA1 field (present study), it is suggested that *Wfs1* mRNA would be detected in interneurons of these strata. However, it is not known whether *Wfs1* mRNA signals are present in interneurons of the pyramidal cell layer. Further studies are required to clarify whether *Wfs1* mRNA is expressed in interneurons of the pyramidal cell layer in the CA1 field.

Functional studies suggested that the septal hippocampus is necessary for spatial learning and memory (Moser et al., 1993; Witter and Amaral, 2004), whereas the temporal hippocampus appears to be essential for normal fear-related behavior in rats (Kjelstrup et al., 2002; Witter and Amaral, 2004). Since *Wfs1* mRNA signals in the CA1 field were observed in both the septal and temporal levels, the *Wfs1* gene might contribute both to spatial learning and memory, and to normal fear-related behavior. In addition, distribution of the signals was not homogeneous in the CA1 field: strong signals were observed in the septal hippocampus while weak-to-moderate signals were seen in the temporal hippocampus (present study). The functional difference between the septal and temporal hippocampi may help to explain the difference in the strength of the signals between the two hippocampi.

4.3.2. PaS

The PaS is one of the parahippocampal areas. In the mouse, *Wfs1* mRNA signals were confined to layers II and III (the external lamina). Afferent fibers to these layers arise from various intrinsic, hippocampal, parahippocampal, cortical, and subcortical structures in the rat (Witter and Amaral, 2004). The PaS gives rise to both intrinsic associational connections (Köhler, 1985; Caballero-Bleda and Witter, 1993), and a commissural projection (Köhler, 1985; Van Groen and Wyss, 1990a). The PaS receives a hippocampal input from the subiculum (Swanson et al., 1978; Köhler, 1985; Van Groen and Wyss, 1990a,c), and a weak parahippocampal input from the entorhinal cortex (Köhler, 1986, 1988; Van Groen and Wyss, 1990a,c). The PaS also receives weak cortical projections from the retrosplenial cortex and the occipital visual cortex (Vogt and Miller, 1983; Van Groen and Wyss, 1990a). Subcortical afferents to the PaS arise from the septum, the endopiriform nucleus (Van Groen and Wyss, 1990a,c; Eid et al., 1996; Behan and Haberly, 1999), amygdala (Van Groen and Wyss, 1990a; Petrovich et al., 1996; Pikkarainen et al., 1999; Kemppainen et al., 2002), and the thalamus. Thalamic inputs to the PaS arise from the anteroventral and anterodorsal nuclei, laterodorsal nucleus, and nucleus reuniens (Herkenham, 1978; Wouterlood et al., 1990; Shibata, 1993; Van Groen and Wyss, 1995). The PaS receives serotonergic projections from the raphe nuclei (Köhler et al., 1981; Köhler and Steinbusch, 1982; Van Groen and Wyss, 1990a,c), and noradrenergic projection from the locus coeruleus (Swanson et al., 1987; Witter and Amaral, 2004).

In addition to receiving afferent fibers, the PaS sends efferent fibers to hippocampal, parahippocampal, and subcortical structures (Witter and Amaral, 2004). The PaS gives rise to hippocampal projections to the dentate gyrus, the hippocampus proper, and to the subiculum (Köhler, 1985; Van Groen and Wyss, 1990a). It sends parahippocampal projections to the presubiculum (Köhler, 1985; Van Groen and Wyss, 1990a) and to the entorhinal cortex (Köhler, 1985; Van Groen and Wyss, 1990a; Caballero-Bleda and Witter, 1993), and gives rise to a modest thalamic projection to the anterodorsal nucleus. This nucleus is the exclusive target of the extrahippocampal projections in the rat PaS (Van Groen and Wyss, 1990a; Witter and Amaral, 2004). As described above, the PaS is involved in several neuronal relays. Probably the most unique characteristic of the PaS is its relay from the anterior thalamic nucleus to the hippocampal formation. This relay provides a route by which thalamic input might influence very early stages of hippocampal information processing (Witter and Amaral, 2004). The *Wfs1* gene possibly contributes to this information processing.

4.3.3. Entorhinal cortex

4.3.3.1. Fiber connections of the superficial layers of the entorhinal cortex. The entorhinal cortex (MEA and LEA) is a part of the parahippocampal cortex. According to the review by Witter and Amaral (2004), fibers of the so-called perforant pathway take their origin mainly from entorhinal-cortical neurons located in layers II and III, where *Wfs1* mRNA signals were observed in the mouse. These layers receive inputs from a variety of cortical structures including the ipsilateral and contralateral entorhinal cortex (Burwell and Amaral, 1998b). Extrinsic cortical afferents to the superficial layers originate from the hippocampal and parahippocampal regions. Hippocampal fibers to the layers arise from the subiculum, and parahippocampal afferents originate from the perirhinal and postrhinal cortices, the presubiculum (Naber et al., 1997; Burwell and Amaral, 1998a,b), and from the PaS (Köhler, 1985; Van Groen and Wyss, 1990a; Caballero-Bleda and Witter, 1993). Finally, a substantial input to the superficial layers originates from the olfactory structures, in particular from the olfactory bulb, the anterior olfactory nucleus, and the piriform cortex (Haberly and Price, 1978; Kosel et al., 1981). In addition, the superficial layers receive subcortical afferents from the telencephalon, the thalamus, the hypothalamus, and the brainstem. Telencephalic inputs arise from the medial septal nucleus, nucleus of the diagonal band, and from the amygdala (Price et al., 1987; Pitkänen et al., 2000). The major thalamic input originates from nucleus reunions (Herkenham, 1978; Wouterlood et al., 1990; Wouterlood, 1991). The hypothalamic input arises from the supramammillary nucleus (Haglund et al., 1984). The brainstem input originates from the ventral tegmental area, the central and dorsal raphe nuclei (Azmitia and Segal, 1978; Köhler and Steinbusch, 1982), locus coeruleus (Moore et al., 1978), and from nucleus incertus, a CRH (corticotropin releasing hormone) receptor-rich nucleus (Goto et al., 2001; Witter and Amaral, 2004).

In addition to these afferent connections, the superficial layers have efferent connections not only with the hippocampal formation (the perforant pathway), but also with parahippocampal, limbic, paralimbic, and olfactory regions of the cortex (Insausti et al., 1997) and with the septal region (Alonso and Köhler, 1984). Perforant path fibers terminate in the dentate gyrus, the CA3 and CA1 fields, and in the subiculum (Witter and Amaral, 2004), and the perforant pathway is most likely glutamatergic (Fonnum,

1970). Parahippocampal projections from the superficial layers terminate in the presubiculum, the PaS (Köhler, 1986, 1988; Van Groen and Wyss, 1990a,c), and in perirhinal area 35 (Insausti et al., 1997; Burwell and Amaral, 1998a). The superficial layers emit projections to the infralimbic cortex, the ventral taenia tecta, the prelimbic, orbitofrontal, and agranular insular cortices (Wyss and Van Groen, 1992; Condé et al., 1995; Insausti et al., 1997), and the olfactory area (de Olmos et al., 1978; Insausti et al., 1997). Additionally, many layer II neurons in the MEA project to the septal region (Alonso and Köhler, 1984; Witter and Amaral, 2004). Thus, it is possible that *Wfs1* mRNA-hybridized cells in layers II and III of the entorhinal cortex are involved in a wide variety of neuronal relays through the perforant pathway described above. Since neurons in these layers are key elements in the temporal lobe memory system (Klink and Alonso, 1997), the *Wfs1* mRNA-hybridized cells contribute to learning and memory. However, it is unclear whether majority of perforant pathway neurons in these layers express *Wfs1* mRNA. Further studies by using tract-tracing methods are required to clarify the fiber connections of *Wfs1* mRNA-hybridized neurons in the entorhinal cortex. Such studies will uncover whether the *Wfs1* mRNA-hybridized cells contribute to learning and memory as projection neurons (perforant pathway neurons) or interneurons.

4.3.3.2. The islet of cells in layer II of the MEA. The present study demonstrated the islet of cells in layer II of the mouse MEA. A majority of the cells in the islet were strongly hybridized with *Wfs1* mRNA. This evidence is supported by the finding that highly Wfs1-positive cell clusters were distributed in the mouse MEA (Luuk et al., 2008; Kawano et al., unpublished observations). Although Woznicka et al. (2006) demonstrated that "distinct spherical groups of small cells are situated at the border of layer I/II" in the caudal part of the canine MEA, there have been few descriptions of the islet in both the mouse and the rat (Insausti et al., 1997; van Groen, 2001; Witter and Amaral, 2004). Further studies are required to clarify hodological, neurophysiological, histochemical, and immunohistochemical details of the islet. In such studies, *Wfs1* mRNA will be a useful marker for the islet.

4.3.3.3. A small number of Wfs1 mRNA signals in layer II of the LEA. A laminar distribution of *Wfs1* mRNA and protein in layer II was present in most of the mouse cortical areas (Kawano et al., 2008; Luuk et al., 2008; Kawano et al., unpublished observation) as described in the rat (Takeda et al., 2001). In the LEA, *Wfs1* mRNA signals were observed in layer III, however, only a small number of the signals was detected in layer II. This evidence suggests that the laminar distribution of *Wfs1* mRNA signals in the LEA is unique to that in the multi-layered cortex. Thus *Wfs1* mRNA might be a useful marker to distinguish the LEA from other cortical areas including the MEA.

4.4. Facial nucleus

In the facial nucleus, the pattern of change in the strength of *Wfs1* mRNA signals differed between the 7NM (type 1b) and the 7NL (type 2a). This difference might be attributable to the myotopical organization in the nucleus. The facial nucleus in rodents is myotopically organized from birth to adulthood: neurons in the 7NM innervate the auricular muscles, whereas those in the 7NL send their axons to muscles in the orbital region, the perioral region, and in the proboscis (muscles involved with orofacial function) (Ashwell, 1982; Ashwell and Watson, 1983; Travers, 2004). It is not known why the type 1b pattern is seen in the 7NM, however, it is possible that the type 2a pattern in the 7NL is attributable to the orofacial function especially feeding, since the same pattern of change (type 2a) was seen in the Mo5 (motor nucleus of the trigeminal nerve) and in the 12N (hypoglossal nucleus), which play important roles in feeding.

4.5. Diabetes insipidus

Arginine vasopressin-synthesizing neurons are distributed in the SO (supraoptic nucleus) and the PVNm (magnocellular part of the paraventricular hypothalamic nucleus) (Armstrong, 2004). *Wfs1* mRNA signals in these nuclei showed the type 2b pattern (Figs. 1, 3G–L; Table 1). This finding suggests that the diabetes insipidus in Wolfram syndrome patients is attributable to dysfunctional neurons in these nuclei resulting from loss-of-function mutations in the *WFS1* gene.

Neuropathological studies showed loss of neurons in the SO and in the paraventricular hypothalamic nucleus (Genís et al., 1997; Shannon et al., 1999). In addition, Gabreëls et al. (1998) examined brains of three Wolfram syndrome patients by using immunohistochemistry for both the vasopressin and for the vasopressin precursor, and described in the patients with diabetes insipidus, not only a loss of the vasopressin in neurons of the paraventricular hypothalamic nucleus, but also a defect in processing of the vasopressin precursor in this nucleus. Thus, the WFS1 protein may function in the survival of neurons and in vasopressin precursor-processing from birth to early adulthood in the SO and/or the PVNm.

4.6. Sensorineural hearing loss

The *WFS1* gene is responsible for both sensorineural deafness in Wolfram syndrome patients (Minton et al., 2003) and autosomal dominant low frequency sensorineural hearing loss (Bespalova et al., 2001; Young et al., 2001). In the mouse brain, *Wfs1* mRNA signals in the cochlear nucleus and inferior colliculus showed the type 2b pattern, and those in the auditory cortex, the type 1c or 3b pattern. In the cochlea, Wfs1 protein was invariably expressed in inner hair cells and spiral ganglion cells from birth to postnatal day 35 (Cryns et al., 2003). Thus, it is suggested that the *Wfs1* gene contributes to both the development and maintenance of cells in the auditory system including the cochlea. It is also suggested that not only dysfunctional inner ear cells but also dysfunctional neurons in the auditory-related structures of the brain attribute to both the sensorineural deafness in Wolfram syndrome patients and autosomal dominant low frequency sensorineural hearing loss.

4.7. Psychiatric symptoms in Wolfram syndrome patients

Swift et al. (1990) reported that 41 of 68 Wolfram syndrome patients (60%) had episodes of severe depression, psychosis, or organic brain syndrome, as well as impulsive verbal and physical aggression. These symptoms were very severe in 17 patients (25%), of whom 12 required admission to a psychiatric hospital and 11 attempted suicide. Based on this evidence, they proposed that the *WFS1* gene predisposed homozygotes to psychiatric illness (Swift et al., 1990). Subsequently, molecular neuropsychiatric studies suggested a role for the *WFS1* gene in the pathophysiology of impulsive suicide (Sequeira et al., 2003), and an association between mutations of the *WFS1* gene and hospitalization for psychiatric illness (Swift and Swift, 2005). In addition, the *Wfs1* gene was suggested to be a putative biomarker for post-traumatic stress disorder by a behavioral study using rats (Kesner et al., 2007), and the *Wfs1* knockout mouse showed bipolar disorder-like behavioral phenotypes, such as retardation in emotionally triggered behavior, decreased social interaction, and altered behavioral despair depending on experimental conditions (Kato

et al., 2008). Conversely, several molecular neuropsychiatric studies have found no evidence of a supporting role for the *WFS1* gene in psychiatric disorders, particularly major depression and bipolar disorder (Furlong et al., 1999; Evans et al., 2000; Middle et al., 2000; Ohtsuki et al., 2000; Kato et al., 2003; Kawamoto et al., 2004). As described here, it is not known whether mutations of the *WFS1* gene contribute significantly to the incidence of psychiatric illness. The present study showed that weak *Wfs1* mRNA signals were distributed in the raphe nuclei and nucleus coeruleus from birth to early adulthood. It is possible that the functions of the raphe nuclei and of the nucleus coeruleus in Wolfram syndrome patients are impaired by loss-of-function mutations in the *WFS1* gene. The dysfunction may predispose the patients to major depression and bipolar disorder, since these nuclei are strongly related to these mood disorders (Kandel, 2000). In addition, the present study demonstrated that strong-to-moderate *Wfs1* mRNA signals were widely distributed in the limbic structures including the hippocampus and the amygdala, and in the rostral part of the cerebral cortex from P14 to early adulthood. It is possible that the psychiatric symptoms in Wolfram syndrome patients are attributable to dysfunctional neurons in these structures arising from loss-of-function mutations in the *WFS1* gene.

4.8. Relationship between Wfs1 mRNA expression and neuroradiological and neuropathological evidence

Neuroradiological (Rando et al., 1992; Scolding et al., 1996; Ito et al., 2007) and neuropathological (Genís et al., 1997; Shannon et al., 1999) examinations have been carried out in brains of Wolfram patients. The principal findings of these examinations were brainstem atrophy, cerebellar atrophy, and optic atrophy. Mild atrophic changes in the cerebral cortex and hypothalamus were also described. The present study showed that strong-to-moderate *Wfs1* mRNA signals were widely seen in the limbic structures (e.g. CA1, MEA, LEA, PaS, S, Tu, BSTL, IPAC, and Ce) from P7 to early adulthood. However, these structures were not affected in Wolfram syndrome patients (Genís et al., 1997; Shannon et al., 1999). Although *Wfs1* mRNA signals in the cerebellar cortex were weak from P4 to early adulthood (type 2b), cerebellar atrophy was demonstrated in Wolfram syndrome patients (Rando et al., 1992; Scolding et al., 1996; Genís et al., 1997; Shannon et al., 1999; Ito et al., 2007).

To reconcile the results with the neuroradiological and neuropathological evidence, the following possible interpretations are offered. In the cerebellum, functions of the WFS1 protein are essential for the survival of neurons expressing weak *WFS1* mRNA signals. In the limbic structures, functions of the WFS1 protein are not necessary for the survival of neurons expressing strong-to-moderate *WFS1* mRNA signals and/or functions of the mutant WFS1 protein are counteracted in these neurons by 'functionally-related proteins of WFS1 (WFS1-frps)', which compensate for functions of the normal WFS1 protein. Thus pathological changes do not occur in the limbic structures, but do occur in the cerebellum.

Interestingly, several nuclei potentially relevant to the symptoms of Wolfram syndrome, such as the SO and PVNm, potentially relevant to diabetes insipidus; the Co and IC, potentially relevant to sensorineural hearing loss; and the LC and raphe nuclei, potentially relevant to psychiatric symptoms, also showed the type 2b pattern the same as the cerebellum. These results support the notion that functions of the WFS1 protein are essential for the survival of neurons expressing weak *WFS1* mRNA signals in symptom-relevant nuclei, the WFS1-frps are not expressed in the neurons, and these factors lead to pathological changes in the symptom-relevant nuclei of Wolfram syndrome patients.

4.9. Conclusion

There were three patterns of change in the strength of *Wfs1* mRNA signals in each of the mouse brain structures during the postnatal development. Out of the three patterns, several nuclei potentially relevant to the symptoms of Wolfram syndrome showed the type 2b pattern, in which the signals were weak and of a relatively constant strength during development. Based on these results, the present study provided a hypothesis that functions of the WFS1 protein are essential for the survival of neurons expressing weak *WFS1* mRNA signals in symptom-relevant nuclei, the WFS1-frps are not expressed in the neurons, and these factors lead to pathological changes in the symptom-relevant nuclei of Wolfram syndrome patients. To test this hypothesis experimentally, the availability of the *Wfs1* knockout mouse could offer opportunities for further investigation. These studies in the next step are necessary to determine the exact physiological role of the Wfs1 protein in the brain, and to obtain more insights into its pathophysiological roles in the endocrinological, otological, neurological, and psychiatric symptoms of Wolfram syndrome.

Acknowledgements

The first and corresponding author, June Kawano, thanks Professor Shiro Nakagawa (Laboratory for Neuroanatomy, Department of Neurology, Kagoshima University Graduate School of Medical and Dental Sciences) for encouragement and for valuable discussions. This study was supported in part by a Grant-in-aid for Scientific Research (C) (15591228 to J.K.) from The Japan Society for the Promotion of Science (JSPS), a Grant-in-aid for Scientific Research on Priority Areas (19040020 to K.S.) from The Ministry of Education, Culture, Sports, Science and Technology (MEXT), and in part by Kodama Memorial Fund Medical Research (2006-100 to J.K.).

References

Alonso, A., Köhler, C., 1984. A study of the reciprocal connections between the septum and the entorhinal area using anterograde and retrograde axonal transport methods in the rat brain. J. Comp. Neurol. 225, 327–343.
Amaral, D.G., Dolorfo, C., Alvarez-Royo, P., 1991. Organization of CA1 projections to the subiculum: a PHA-L analysis in the rat. Hippocampus 1, 415–435.
Armstrong, W.E., 2004. Hypothalamic supraoptic and paraventricular nuclei. In: Paxinos, G. (Ed.), The Rat Nervous System. third ed. Elsevier Academic Press, San Diego, pp. 369–388.
Ashwell, K.W., 1982. The adult mouse facial nerve nucleus: morphology and musculotopic organization. J. Anat. 135, 531–538.
Ashwell, K.W., Watson, C.R., 1983. The development of facial motoneurones in the mouse—neuronal death and the innervation of the facial muscles. J. Embryol. Exp. Morphol. 77, 117–141.
Azmitia, E.C., Segal, M., 1978. An autoradiographic analysis of the differential ascending projections of the dorsal and median raphe nuclei in the rat. J. Comp. Neurol. 179, 641–667.
Barrett, T.G., Bundey, S.E., Macleod, A.F., 1995. Neurodegeneration and diabetes: UK nationwide study of Wolfram (DIDMOAD) syndrome. Lancet 346, 1458–1463.
Behan, M., Haberly, L.B., 1999. Intrinsic and efferent connections of the endopiriform nucleus in rat. J. Comp. Neurol. 408, 532–548.
Bespalova, I.N., Van Camp, G., Bom, S.J., Brown, D.J., Cryns, K., DeWan, A.T., Erson, A.E., Flothmann, K., Kunst, H.P., Kurnool, P., Sivakumaran, T.A., Cremers, C.W., Leal, S.M., Burmeister, M., Lesperance, M.M., 2001. Mutations in the Wolfram syndrome 1 gene (*WFS1*) are a common cause of low frequency sensorineural hearing loss. Hum. Mol. Genet. 10, 2501–2508.
Burwell, R.D., Amaral, D.G., 1998a. Perirhinal and postrhinal cortices of the rat: interconnectivity and connections with the entorhinal cortex. J. Comp. Neurol. 391, 293–321.
Burwell, R.D., Amaral, D.G., 1998b. Cortical afferents of the perirhinal, postrhinal, and entorhinal cortices of the rat. J. Comp. Neurol. 398, 179–205.
Caballero-Bleda, M., Witter, M.P., 1993. Regional and laminar organization of projections from the presubiculum and parasubiculum to the entorhinal cortex: an anterograde tracing study in the rat. J. Comp. Neurol. 328, 115–129.
Cano, A., Rouzier, C., Monnot, S., Chabrol, B., Conrath, J., Lecomte, P., Delobel, B., Boileau, P., Valero, R., Procaccio, V., Paquis-Flucklinger, V., Vialettes, B., 2007. Identification of novel mutations in *WFS1* and genotype–phenotype correlation in Wolfram syndrome. Am. J. Med. Genet. A 143A, 1605–1612.